UiT The Arctic University of Norway

Department of Electrical Engineering

Study of Inter Area Oscillations Using Phasor Measurement Units

Improving damping of inter-area oscillations with the implementation of remote signals from Phasor Measurement Units

Henrik Olsen
Supervisor: Charu Sharma

Master's thesis in Electrical Engineering…ELE-3900…May 2021

Table of Contents

List of Tables

List of Figures

Important glossary

AVR Automatic Voltage Regulator - Excitation control equipped on the generator to keep a fixed terminal voltage

FACTS Flexible Alternating Current Transmission System - alternating current transmission systems incorporating power-electronics based and other static controllers to enhance control ability and power transfer ability.

PMU Phasor Measurement Units- a device that produces Synchronized Phasor, Frequency, and Rate of Change of Frequency (ROCOF) estimates from voltage and/or current signals and a time synchronizing signal

POD Power Oscillation Damper - a device equipped to the FACTS which its purpose is to provide an electrical torque in phase with the speed deviation to ensure improved damping torque

PSAT Power System Analysing Toolbox - a Matlab toolbox for electric power system analysis and simulation.

PSS Power System Stabilizer - a device equipped to the AVR which its purpose is to provide an electrical torque in phase with the speed deviation to ensure improved damping torque

SVC Static VAR Compensator - a set of FACTS devices for providing fast-acting reactive power on high-voltage electricity transmission networks.

Abstract

Low frequency oscillations in the power system have major repercussions on power system stability and the objective of maximum power transfer. Local and global control strategies have been developed to dampen and impede these oscillations. A modern local control strategy is supplying the automatic voltage regulation (AVR) of the generator with a power system stabilizer (PSS). Modern global control strategies include supplying the tie lines with flexible alternating current transmission systems devices (FACTS) and a power oscillation damper (POD).

Including global signals in conjunction with local signals as an input on the generators PSS has been studied [24,25], but follows the same problems as PSSs tuned to enhance damping of the inter-area mode. Once satisfactory results are achieved on the inter-area mode, local modes of the machines involved in the inter-area mode tend to become less stable, or unstable. This type of interaction has caused most of the latest problems regarding damping of the inter-area mode with the use of the generators PSS [1,24,25].

The following thesis investigates the impact on inter-area oscillations of including global measurements from phasor measurement units (PMU) in conjunction with local measurements as an input signal on a FACTS-device installed on the tie-line between two interconnected areas. A remote measurement feedback controller has been designed, tuned, and placed on the two-area; four-machine system, created for studying inter-area oscillations. Phasor measurements from optimally located measurement units were shown to improve the damping of the local and inter-area, low-frequency oscillations. The advantages of damping the before-mentioned oscillations were apparent through the ability to increase the power transfer capability in the tie-lines between the two areas following the implementation of the control method. The robustness of the suggested control method was analyzed through a small-signal stability test increasing tie-line power transfer, and a transient stability test using time-domain simulations of a severe fault, more specific a three-phase short circuit on the tie-lines.

1 Introduction and literature review

1.1 Problem statement

Spontaneous low-frequency oscillations formed part of the earliest power system stability problems, until the introduction of damper windings on the generators rotor windings. For some time, the problem was disregarded until the power system started to operate closer to its stability limit and the lack of synchronous torque became evident. This led to the introduction of AVRs which improved steady-state stability by increasing synchronizing torque, but at the cost of decreasing damping torque, leading to concerns regarding transient stability. As the power system grew and the construction of immense interconnected systems followed, large quantities of power transmitted over great distances became a concern. Supplementary control strategies like the addition of PSSs to the generators AVR, and later, the installation of FACTS devices, provide the necessity to decrease the impeding effects of low-frequency oscillations, both regarding increased power transfer capacity and increased small-signal, and-transient stability [34].

1.1.1 Present-day solution

Figure. 1 represents the contemporary solution where the FACTS device and power oscillation damper is locally controlled, i.e., respond on local measurements (dashed line) from e.g., bus-voltage, line current, active power, reactive power etcetera.

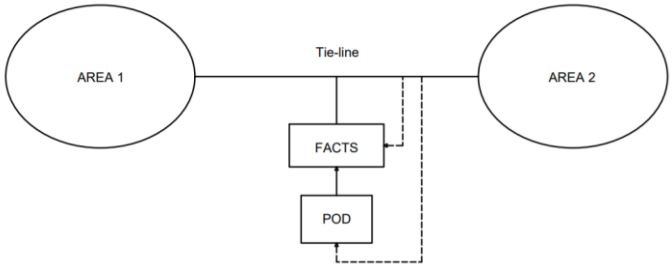

Figure. 1. Present-day solution of FACTS in conjunction with a local input POD.

1.1.2 Suggested solution

A new control scheme is shown in Figure. 2. Like the contemporary solution, the FACTS-device is likewise locally controlled. However, the POD responds to remote measurements provided by PMUs as a substitution for the locally metered input variables for the controls.

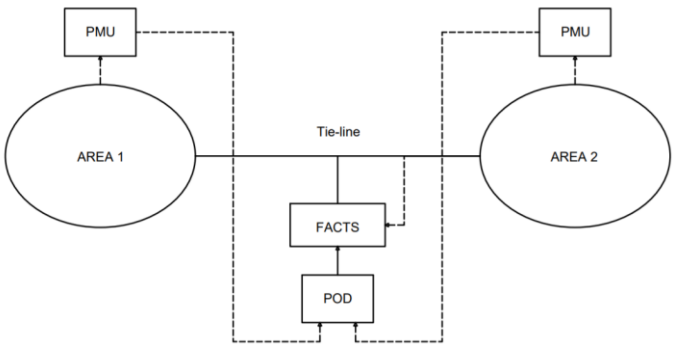

Figure. 2. Suggested solution of FACTS in conjunction with a global input POD.

Other researchers and electric utility companies have investigated the use of PMU since it originated both for identifying inter-area oscillations and including its signals in feedback control. A thyristor-controlled series compensator wide-area damping controller is presented for improving stability based on signals from PMU in [2]. An adaptive phasor power oscillation damping controller which uses wide-area measurement signals from PMU considering time-delay in remote feedback control signals is developed in [3]. A power oscillation damping controller is presented using wide-area measurements from PMU applied to FACTS devices in [4]. A systematic procedure of designing a centralized wide-area damping controller system for inter-area oscillation damping based on PMU signals is presented in [5]. Lastly, a wide-area POD was designed which uses voltage phase angle signals from two distant locations in the Norwegian grid as inputs to the damping controller of a FACTS-device in [6].

1.2 Research goals

This thesis will focus on the design of a PMU-based remote feedback controller for a POD applied on a FACTS-device, as well as its impact on the damping of inter-area oscillations of the two-area, four-machine system. An approach based on linear analysis is developed to determine the placement of the FACTS-device as well as optimal PMU placement and output signal. The proposed solution will be shown to increase joint controllability and observability of the inter-area mode compared to that of a locally controlled FACTS-device with a power oscillation damper. Improvement in small-signal stability in regards to increased power transfer capacity will be demonstrated as well as time-domain simulations showcasing improvement in transient stability following a three-phase short-circuit on the tie lines.

2 Background theory

The impact some of the various phenomena and controls have on damping will be demonstrated in Section. 6, and therefore, it is important to understand the dynamics behind their impact. This section will provide important background theory on both oscillatory behavior in generators, as well as important factors contributing to both positive and negative damping. Information and notations used for this chapter are derived from [25] unless other is stated.

2.1 Understanding oscillations in the power system

Mechanical movement of the generator's rotor is influenced by electromagnetic effects, and depending on the operating state of the generator, this movement varies.

When the turbine and generator inertia rotate without any relative displacement, the natural frequency of 0 Hz occurs on the turbine/generator drive system.

Newtons second law states

$$J\frac{d\omega_n}{dt} + D_d\omega_m = \tau_t - \tau_e \tag{2.1}$$

where J is the total inertia of the rotating system, ω_m is the rotational velocity of the rotor shaft, D_d is the is the damping constant due to mechanical rotational losses from friction and electrical losses from windage. τ_t is the mechanical torque on the turbine, while τ_e is the counteracting electromagnetic torque. This equation shows that any imbalance between the torque components will cause a change in rotational velocity of the rotor shaft. If $\tau_t > \tau_e$ the rotor accelerates, and if $\tau_t < \tau_e$ the rotor deaccelerates. Faraday's law states that to change a flux arbitrarily, infinite voltage must be applied [36]. Therefore, during a disturbance, to keep constant flux linkage, the rotor angle must change. A change in movement requires work to be performed. For rotating systems, work is equal to the torque acting over the angular displacement. This torque is the difference between mechanical and transient electrical torque. Power is the product of torque and velocity. Therefore, the work done by the disturbance in Figure. 3, is given by

$$W_{1-2} = \int_{\hat{\delta}_S}^{\hat{\delta}_S+\Delta\delta_0} [P_{E'}(\delta) - P_m]d\delta = Area(1-2-3) \tag{2.2}$$

where $P_{E'}(\delta)$ is the transient power angle characteristics, P_m is the mechanical power, and $\Delta\delta_0$ is the change in rotor angle. The work done by this area is the systems increase in potential energy following a disturbance. This potential energy provides the impetus required to return the rotor angle to its equilibrium point. At point 2, $\tau_m < \tau_e$, meaning the deacceleration power will reduce the rotor speed and rotor angle. Returning to the equilibrium point (point 1), all potential energy has been converted to kinetic energy. The kinetic energy will now push the rotor past equilibrium point 1, towards point 3. Here $\tau_m > \tau_e$, which means the rotor will accelerate and continue until the work done by the acceleration torque is equal to the previous work done by the deacceleration area. Again, the rotor will continue to accelerate towards point 2 before the cycle continues. In the absence of any damping, these oscillations would be standing, leaving a marginally stable system.

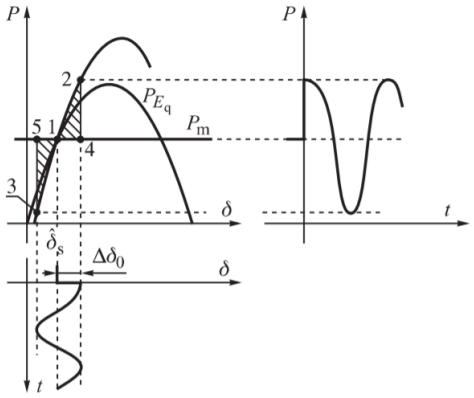

Figure. 3. Standing oscillations following a disturbance for an undamped system [26].

The incremental swing equation for the generator-infinite busbar system is given by

$$M\frac{d^2\Delta\delta}{dt^2} + D\frac{d\Delta\delta}{dt} + K_{E'}\Delta\delta = 0 \tag{2.3}$$

where M is the generator's coefficient of inertia, D is the damping coefficient, and $K_{E'}$ is transient synchronizing power coefficient, meaning the slope of the transient power angle curve $P_{E'}(\delta)$, can be compared with the standard mass-spring-damper-system in Figure. 4, given by

$$m\frac{d^2\Delta x}{dt^2} + c\frac{d\Delta\delta}{dt} + k\Delta x = 0 \tag{2.4}$$

An increase in spring extension Δx is equivalent to an increase in rotor angle $\Delta\delta$. The mass m is equivalent to the inertia coefficient M, which also implies that a greater mass/inertia leads to lower frequencies of oscillatory behavior which will be further discussed in Section. 2.2. The spring's damping coefficient c, is comparable to the generators damping coefficient D. Lastly The springs stiffness k is equivalent to synchronizing power coefficient $K_{E'}$, though the latter is non-linear and depends on the initial angle of the power angle.

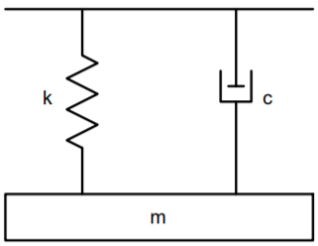

Figure. 4. Mass-spring-damper system.

2.2 Low frequency oscillations

The generator's rotor angle oscillations with frequencies in the region 0.1 to 3.0 Hz, defined by where their location is in the power system characterizes low-frequency oscillations. As stated in Section. 2.1, greater inertia, means lower frequency of oscillations. As the impedances in the tie-lines between two interconnected systems are much greater than the impedances between the generators in each respective area, the inter-area mode of oscillation will "see" the sums of the inertia coefficients of the rotating masses in each system as one and hence the low frequencies of 0.1-0.7 Hz occur. The oscillations represent the swinging between the generators of each respective area. For this reason, the test system used in this study is sufficient for the study of low-frequency oscillations, where each area consists of two large generators. More information about the test system is given in Section. 6. Other oscillatory modes of interest include local plant modes (0.8-1.8 Hz) which is the swinging between generators in one area. Other modes include control modes and torsional modes caused by the interaction between the mechanical and electrical modes of a turbine-generator system. However, the two last-mentioned modes will not be investigated in this thesis. Analysis- and control techniques are discussed in Section. 3 and 4.

2.3 Factors contributing to damping

The power system is a largely underdamped system mainly composed of reactants. This means, once oscillations occur and no additional damping is provided, the oscillations would eventually decay, but over a wide timespan. Once oscillations occur, the system is more vulnerable to additional faults/load changes. This section will provide information regarding naturally occurring damping as well as artificial damping. Phenomena and devices contributing to negative damping will also be discussed.

2.3.1 Damper windings

Damper windings are composed of high resistance/low reactance materials. During rotor oscillations, the rotor speed deviates from synchronous speed. Throughout this period, the flux is not stationary with respect to the rotor, and therefore, currents are induced in the damper windings. Lenz's law states that the direction of the electric current which is induced in a conductor by a changing magnetic field is such that the magnetic field created by the induced current opposes the initial charging magnetic field [35]. This means that the currents induced in the damper windings will oppose the flux change that produced them and therefore contribute to restoring synchronous speed and damp oscillations.

The standard swing equation can be written as

$$M\frac{d^2\Delta\delta}{dt^2} = P_m - [P_e(\delta) + P_D] \tag{2.5}$$

where P_D is the damping power and $M = J\omega_{sm}$, where ω_{sm} is synchronous speed. When the generator experiences a negative speed deviation, i.e., $\omega_{sm} > \omega_m$, the damping power is negative, opposing the electromagnetic power and sifting the $P_E, + P_D$ characteristics downward. For a positive speed deviation, i.e., $\omega_{sm} < \omega_m$, the damping power is positive, assisting the electromagnetic power, shifting the $P_E, + P_D$ characteristics upward. Both incidents are illustrated in Figure. 5.

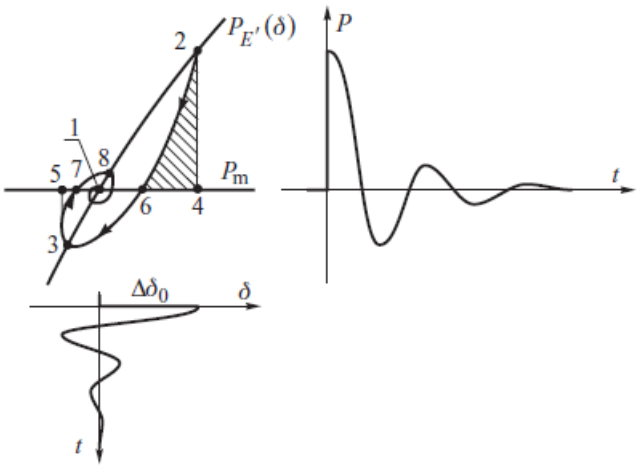

Figure. 5. Decaying oscillations following a disturbance for a damped system [26].

2.3.2 Rotor flux linkage variation

As previous mentioned, a flux linkage cannot change instantly, however, during oscillations as the armature flux enters the rotor windings, the stored magnetic energy dissipates in the resistive components of the rotor. The transient emf E' will therefore change with time.

A vastly simplified, linearized circuit of the generator connected to an infinite busbar with a voltage V_t, through a line with a resistance R_ℓ, and a reactance X_ℓ is given in Figure. 6. A more comprehensive generator modelling explanation is given in Appendix. B and may lead to an easier understanding of this section.

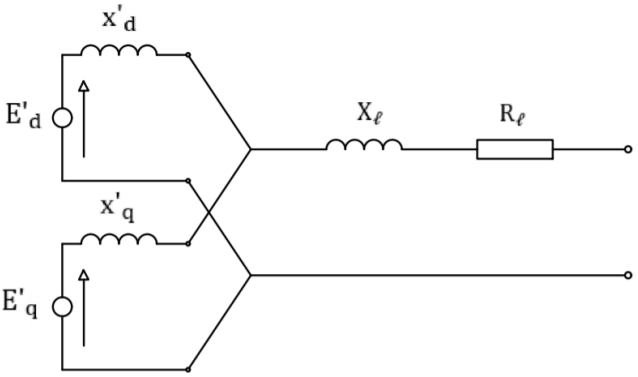

Figure. 6. Simplified synchronous generator operating in transient conditions.

Analyzing the time changes of both the transient emf components E'_d and E'_q is excessive for understanding the effects of rotor flux linkage variation on damping. Therefore, a salient pole machine, without damper windings is considered when $E'_d = 0$, and $E' = E'_q$ so only the flux linkage of the field winding is considered.

Derived from [27], the change in transient emf along the d-axis is given by

$$\Delta E'_q = -\frac{ב_1 ב_2}{1 + ב_1 \tau_{d0} s}\Delta\delta \tag{2.6}$$

where $ב_1$ is an impedance factor that takes into consideration the loading effect of the line impedance and is given by

$$\text{ב}_1 = \frac{1}{1 + \frac{(x_d - x'_d)(x_q + X_\ell)}{R_\ell{}^2 + (x_q + X_\ell)(x'_d + X_\ell)}} \tag{2.7}$$

, and ב_2 is related to the demagnetization effect of the change in rotor angle and is given by

$$\text{ב}_2 = V_t \frac{(x_d - x'_d)\left[(x_q + X_\ell)sin\delta - R_\ell cos\delta\right]}{R_\ell{}^2 + (x_q + X_\ell)(x'_d + X_\ell)} \tag{2.8}$$

with τ_{d0} being the field winding transient time constant.

Studying the frequency response by replacing s with $j\Omega$ in (2.6), it can be seen that $\Delta E'_d$ lead $\Delta\delta$ by $\pi/2$. Obviously $\Delta\delta$ is in phase with the electric power P_e, and $\Delta E'_d$ is in phase with the rotor speed deviation. Figure. 7 shows the effects of flux linkage variation on a synchronous generator without damper windings exposed to a fault leading to oscillations. Now, the disturbance moves the electrical power from point 1-2. The rotor loses speed since $P_m < P_e$, and $\Delta\omega$ becomes negative. The magnetic energy stored in the flux linkage decay with time due to resistive elements in the field- and damper windings, causing the transient emf to decay. Consequently, the rotor motion moves along 2-6 instead of 2-1 as it would if E' was constant since the electrical power is less. The deacceleration area, $Area(2-4-6) < Area(2-4-1)$ which reduces the kinetic energy responsible for the backswing. Going beyond point 6, towards 3, $P_m > P_e$, causing rotor acceleration, meaning, $\Delta\omega$ is positive, which again causes E' to recover. At point 6 E' reaches its pre-disturbance value and $Area(6-3-5) = Area(2-4-6)$. The rotor continues to accelerate and swing back towards the equilibrium point. As the speed deviation continues to increase, so does the transient emf. The acceleration area therefore reduces along with the kinetic energy which is responsible for the forward swing. $Area(6-3-5)$ is the acceleration area and the forward swing ends at point 8. The cycle would repeat with a smaller amplitude of swings, until the oscillations eventually fade.

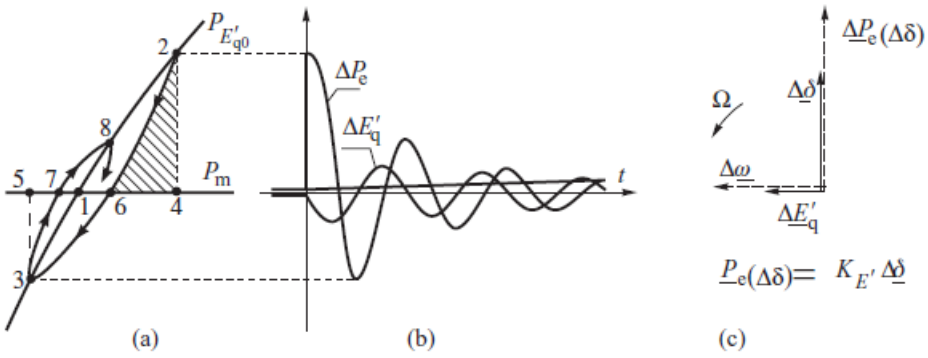

Figure. 7. Including the effect of variation in rotor flux linkage: (a) trajectory of the operating point; (b) time variation of electrical power and transient emf oscillating with the swing frequency; (c) rotating phasors of increments [26].

Taking a closer look at ב_2. In some special cases, the constant becomes negative which implies $\Delta E'$ lies in the opposite direction of $\Delta\omega$. The part of interest in (2.8) is given by

$$" \ (x_q + X_\ell)sin\delta - R_\ell cos\delta \ "$$

For lightly loaded generators, dominated by resistive transmission lines, (2.8) would be negative, leaving $\mathfrak{D}_2$ negative with respect to $\Delta\omega$. Consequently, negative damping is introduced into the system. Contrary to the first case, $\Delta E'$ lags $\Delta\delta$, meaning, during the backswing, the distance from point $2-3$ is shorter than the distance from $3-4$ in Figure. 8. Due to the first law of thermodynamics, the acceleration area cannot be larger than the deacceleration area unless energy is introduced, meaning, since $2-3<3-4$ and $Area(2-3-2')=Area(3-4-4')$, the amplitude of the backswing increases and ΔP_e and $\Delta\delta$ also increases. If the negative damping introduced is larger than the positive damping provided by the damper windings, the generator will lose stability.
The test system used in this thesis does not meet the conditions for this to occur, but it is worth noting for better understanding of Section. 2.3.3 and negative damping in general.

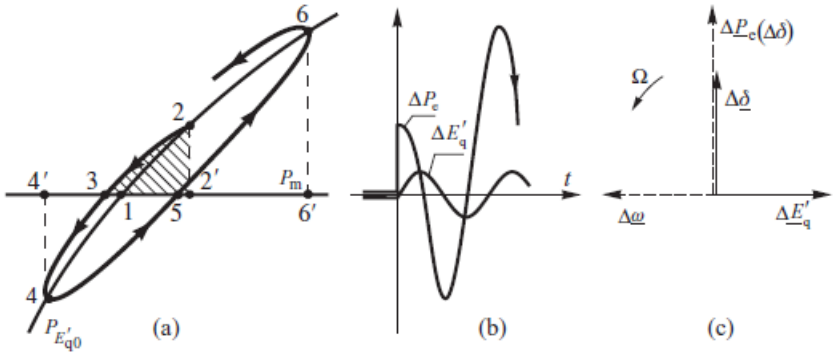

Figure. 8. Negative damping: (a) trajectory of the operating point; (b) time variation of electrical power and transient emf; (c) relative position of phasors of oscillating increments [26].

2.3.3 AVR

Every generator is equipped with an automatic voltage regulator (AVR), accountable for keeping constant terminal voltage, independent of the generator load. This is done by varying the excitation voltage E_f.

2.3.3.1 Direct impact on stability

Figure. 9 shows a generator with constant terminal voltage in steady state, assuming no saliency, and negligible resistance operating on the infinite busbar, as well as its phasor diagram.

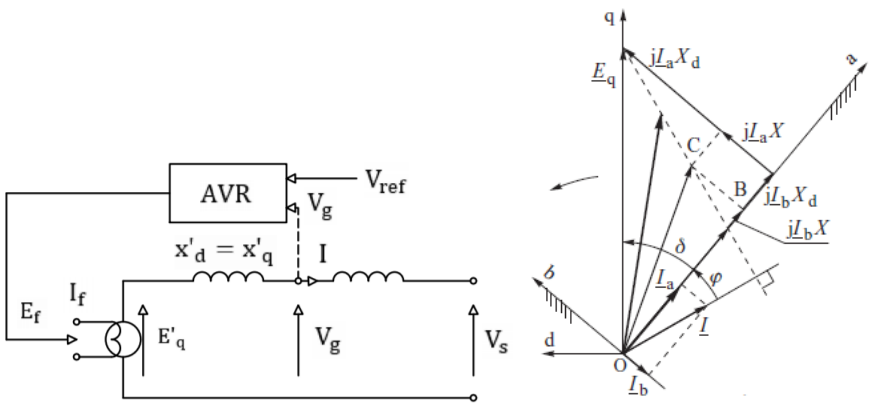

Figure. 9. Generator operating on the infinite busbars: (a) schematic and equivalent circuit; (b)phasor diagram in the (d, q) and (a, b) reference frames. (b) originates from [26].

Applying mathematical geometrical principles to the triangle OBC gives

$$\left(E_{qa}+\frac{x_d}{X}V_s\right)^2+{E_{qb}}^2=\left[\frac{x_d+X}{X}V_g\right]^2 \tag{2.10}$$

Mathematical principles say (2.10) is describing a circle with radius $\rho=\frac{x_d}{X+1}$, located at the axis along V_s (a-axis), with a distance from the center $A=-\frac{x_d V_s}{X}$.

Through some mathematical steps found in [26], the power angle equation is derived

$$P_{vg}(\delta)=\frac{V_s}{x_d+X}sin\delta\sqrt{\left(\frac{x_d+X}{X}V_g\right)^2-\left(\frac{x_d}{X}V_s sin\delta\right)^2}-\frac{1}{2}\frac{x_d}{X}\frac{{V_s}^2}{x_d+X}sin2\delta \tag{2.11}$$

Comparing the power angle characteristics for a round rotor generator with constant emf and a generator equipped with an AVR is shown in Figure. 10, as well as its circle diagram. The amplitude of the power angle characteristics is increased in $P_{vg}(\delta)$ compared to $P_{Eq}(\delta)$. The negative $sin2\delta$ component in (2.11) causes the peak of the curve to occur at a $\delta>\frac{\pi}{2}$. When the electric load of the generator increases, the armature current also increases, which in turn causes a voltage drop in the network reactance, which sequentially leads to a decreased generator voltage. The AVR increases excitation voltage through increased field current until the voltage error is diminished. This is the characteristics of an AVR and the reasoning for the distorted characteristics for $P_{vg}(\delta)$.

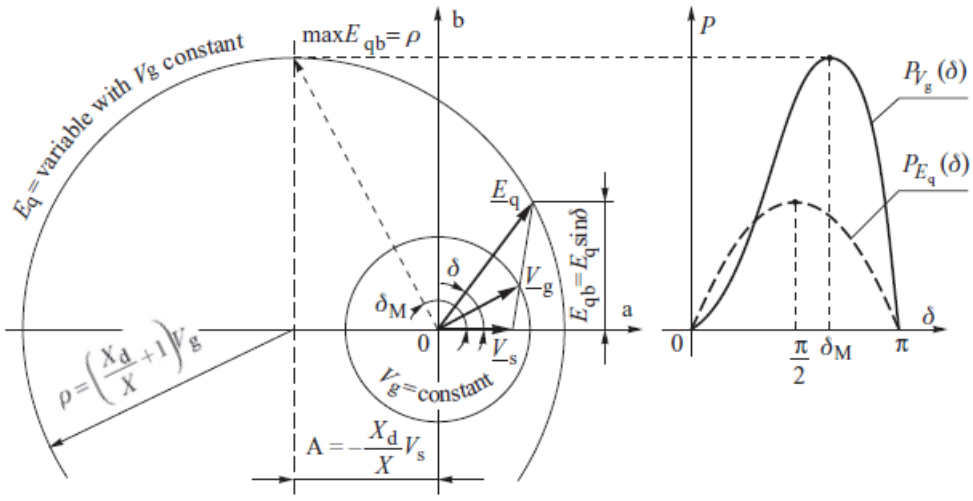

Figure. 10. Circle diagrams and the power–angle characteristics for the round-rotor generator operating on the infinite busbars [26].

If a fast-acting AVR interfere during the transient state of the generator, it can lead to instability. An example of this is shown in Figure. 11. During a swing when the electrical power is greater than the pre-fault power, the AVR will reduce excitation emf to lower the terminal voltage. This will in turn lower the amplitude of the power angle characteristics, leaving a reduced available deacceleration area, causing greater room for instability.

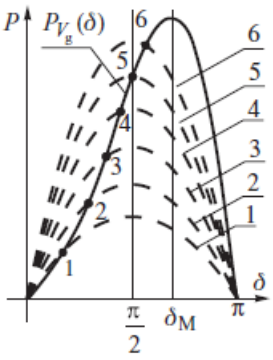

Figure. 11. Power-angle characteristics for a generator applied with AVR [26].

2.3.3.2 Impact on damping

As previously mentioned, when a fault occurs, the rotor angle changes. An increase in rotor angle causes an approximately proportional decrease in generator voltage. The AVR will therefore see a voltage error given by

$$\Delta V = -\frac{\partial V_g}{\partial \delta}\Delta\delta \tag{2.12}$$

The AVR increases the excitation emf which introduces another component affecting the transient emf, and is given by

$$\Delta E_{q(\Delta E_f)} = \frac{\beth_2}{1+\beth_2\tau_{d0}s}\Delta E_f \tag{2.13}$$

For most cases except lightly loaded generators, dominated by resistive transmission lines, this component is positive, meaning $\Delta E_{q(\Delta E_f)}$ lags the changes $\Delta\delta$ by $\frac{\pi}{2}$. Section. 2.3.2 showed how this introduces negative damping into the system, although it is also showed in Figure. 12.

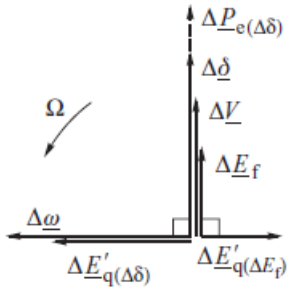

Figure. 12. Phasors of increments rotating with the swing frequency for the AVR proportional system [26].

In addition to the field winding, the damper winding is also affected by the AVR. From Figure. 13, the damper winding along the d-axis lies in the same direction as the excitation flux from the field winding. The damper- and field windings are therefore magnetically linked (Appendix. B). The damper winding resistance is therefore fed by a change in field winding emf. Figure. 13 also shows the equivalent circuit. The current $i_{D(\Delta E_f)}$ lags the change in emf and will therefore introduce negative damping into the system, contrary to the positive damping component introduced by the resistance, discussed in Section. 2.3.1.

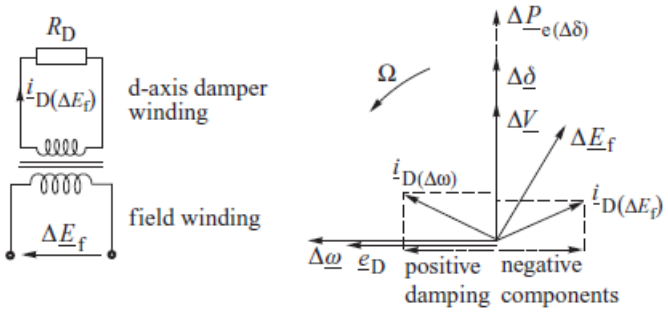

Figure. 13. Phasor diagram of increments oscillating with the swing frequency for the damper windings: (a) field and damper windings as a transformer; (b) natural and artificial damping [26].

2.3.4 Power system stabilizers

Enhancing power system stability can be done by applying additional supplementary control to the AVR by implementing PSS.

When the generator is in the transient state and the rotor speed variations cause the voltage error to oscillate, the PSSs task is to add a voltage signal in phase with $\Delta\omega$ which compensates for the voltage error oscillations. The voltage provided by the PSS should be shifted by π from the voltage error oscillations and at least zero out the negative damping induced by the AVR. If the voltage provided by the PSS is greater than the magnitude of the voltage error oscillations, positive damping is induced as shown in Figure. 14 b.

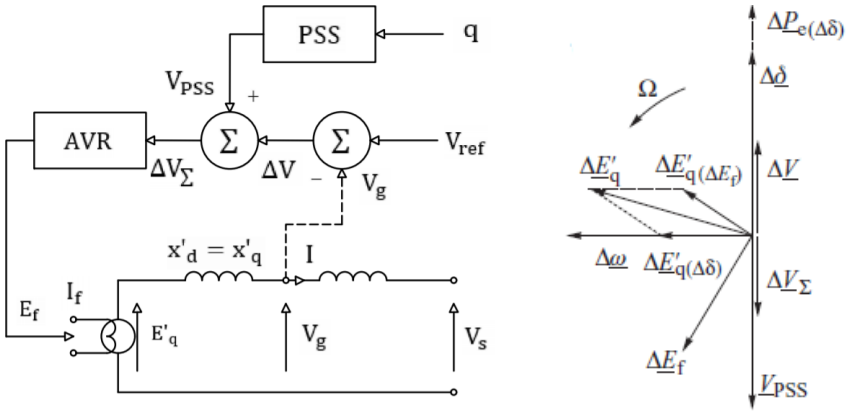

Figure 14. Supplementary control loop for the AVR system: (a) block diagram circuit; (b) phasor diagram. (b) originated from [26].

2.3.5 FACTS devices

To understand how power swings can be damped by changing the parameters in the transmission line, one must understand how the line impedance affects damping power. This is best done by deriving an equation for the damping power. To shorten the process, a simplified generator is considered where it is assumed no resistances except damper windings, damping is provided only by the damper windings, there is no leakage reactance, and excitation does not affect damping. Its equivalent circuit is shown in Figure. 15.

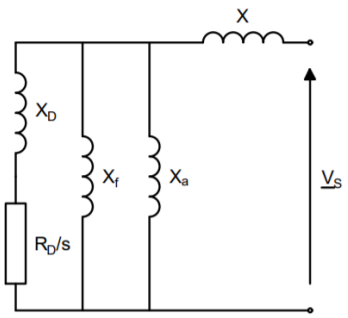

Figure. 15. Simplified equivalent circuit for a synchronous generator operating as induction machine.

X is the network reactance consisting of the generators step-up transformer, the system reactance and transmission line reactance. The transient and subtransient reactants are approximately given by

$$x'_d \cong \frac{1}{\frac{1}{X_f}+\frac{1}{X_a}}, x''_d \cong \frac{1}{\frac{1}{X_f}+\frac{1}{X_a}+\frac{1}{X_D}} \tag{2.13}$$

where X_f is the field winding reactance, X_a is the armature reaction reactance, and X_D is the damper winding reactance.

The deviation can be found in [28] and the equation for damping power with the previous mentioned conditions are given by

$$P_D = V_s^2 \left[\frac{x'_d - x''_d}{(X + x'_d)^2} \frac{x'_d}{x''_d} \frac{\tau''_d \Delta\omega}{1 + (\tau''_d \Delta\omega)^2} \sin^2\delta + \frac{x'_q - x''_q}{\left(X + x'_q\right)^2} \frac{x'_q}{x''_q} \frac{\tau''_q \Delta\omega}{1 + \left(\tau''_q \Delta\omega\right)^2} \cos^2\delta \right] \tag{2.14}$$

where τ''_d and τ''_q is the d- and q-axis subtransient short circuit time constant.

Of interest, the extent of impact the network reactance has on the damping power is rather significant since its squared value appears in the denominator.

FACTS devices providing reactive power, i.e., providing a "negative" X can cancel out this reactance and thereby help damp power oscillations by increasing damping power.

Additional to lowering line impedance, by applying the FACTS device with a POD which has a similar structure to that of the PSS (see Section 5.3 and 5.4), its semiconductor switching devices can be modulated to provide a voltage in phase with $\Delta\omega$, which provides electrical damping power. After the oscillations are damped, the thermal limits of the tie-lines may be approached. This technology is useful for large power transfer and line outages. The impact of these two mechanisms will be demonstrated to enhance stability of the inter-area mode in Section. 6.3 and 6.4.

2.4 Phasor measurement unit (PMU)

A phasor measurement unit is a device used for estimating electric phasor quantities like currents and voltages. The synchronization of the numerous measurements from remote locations on the grid is provided by GPS or IEEE 1588 precision time protocol. These measurements can also be used for estimating other variables like power flow or frequency. Figure. 16 displays the basic functioning of a PMU. The numerous applications of these measurements include power system monitoring, transient stability control, state estimation, etcetera. The objective of this thesis is not to serve as an extensive review of the technology and application but rather an investigation of the usage of its output signals. The state-of-the-art of this technology and application are well documented [29] and will not be further discussed.

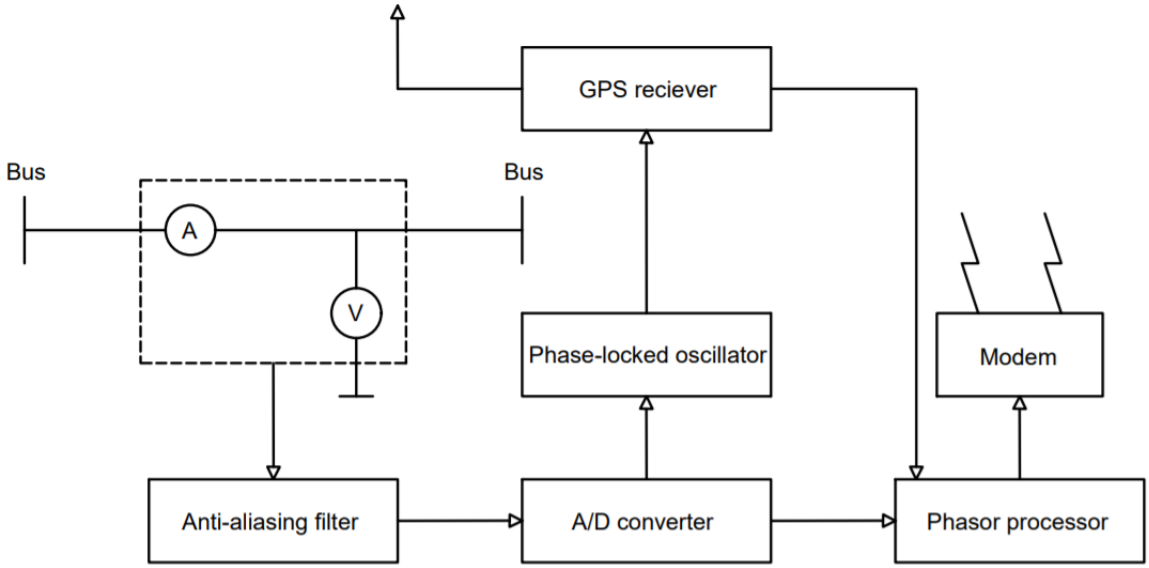

Figure. 16. block diagram showcasing the working of phasor measurement units.

2.5 Generator theory

Synchronous machine theory is of great importance for grasping the effects each control strategy and phenomena have on damping. The large number of circuits involved, and the fact that mutual and self-inductances of the stator and rotor circuits vary with rotor position complicates the synchronous machine equations. By establishing three sets of fictitious perpendicular windings representing the armature of the synchronous generator from the dq-frame, all elements of inductance become constant and independent of time as the dq-frame is constantly rotating with the magnetic rotor axis. Understanding the relationship between the generator in the stator- and dq-reference frame is of great importance as the dq-reference frame is required for state-space representation. Studying the synchronous generator through its machine equations gives a clearer insight of the dynamics behind oscillatory behavior and is given in Appendix B. Readers not acquainted with the topic are referred there.

3 Power system stability

The concept of stability must be outlined to evidently determine the objectives of this thesis. The information and notations are gathered from [1], unless other is stated.

3.1 Definition of stability in power systems

Small-signal stability is the capability of the power system to preserve its synchronism under small disturbances. Reasoning for such disturbances were outlined in Section. 2. The disturbances are deemed sufficiently small for linearization of system equations to be permitted for objectives of analysis.

Transient stability is the capability of the power system to preserve its synchronism under severe transient disturbances such as short circuits and phase-to-ground faults. As the change of rotor angle and speed following transient disturbances often is significant, analysis of such faults requires non-linear analysis.

As low frequency oscillations generally are caused by small disturbances like load changes, and results in small, steady increases in rotor angle the problem usually is analyzed through linearization. The eigenvectors of the system state matrix yield indices that offer identification and categorization information. These indices include participation factors, mode shape, residues, observability, and controllability.

Since control strategies must perform adequate for both small-signal- and transient stability, and the last-mentioned issue introduces non-linear oscillations which requires analyzing techniques beyond this thesis for exact representation. In this thesis, time-domain simulations will be used, and deemed sufficient.

3.2 State space representation

The problem related to low frequency oscillations is analyzed from a small-signal stability perspective. The power system can be described by a set of state equations that are linearized. In this thesis, a search is executed for local- and inter-area modes of oscillation. The reasoning for this is to identify the different control strategies impact on stability and frequency of the above-mentioned modes. Linearization of the generator, supplementary control units, and the FACTS device are found in Section. 5.

3.3 State space model

The behavior of a power system or other dynamic systems, may be described by a set of n, first order nonlinear differential equations of the following form:

$$\dot{\mathbf{x}}_i = \mathbf{f}_i(x_1, x_2, \cdots, x_n; u_1, u_2, \cdots, u_r; t) \qquad i = 1,2, \cdots, n \tag{3.1}$$

Where n is the order of the system and r is the number of inputs. Using vector-matrix notation, this can be written in the subsequent form:

$$\dot{\mathbf{x}} = \mathbf{f}(\mathbf{x}, \mathbf{u}, \mathbf{t}) \tag{3.2}$$

where

$$\mathbf{x} = \begin{bmatrix} x_1 \\ x_2 \\ \vdots \\ x_n \end{bmatrix} \quad \mathbf{u} = \begin{bmatrix} u_1 \\ u_2 \\ \vdots \\ u_r \end{bmatrix} \quad \mathbf{f} = \begin{bmatrix} f_1 \\ f_2 \\ \vdots \\ f_n \end{bmatrix} \tag{3.3}$$

x is the state vector and contains the state variables of the power system and **u** contains the inputs of the system. $\dot{\mathbf{x}}$ is the derivative of a state variable with respect to time. Since the derivatives of the state variables are not explicit functions of time, (3.3) is simplified to

$$\dot{\mathbf{x}} = \mathbf{f}(\mathbf{x}, \mathbf{u}) \tag{3.4}$$

Relating the inputs to the outputs and state variables can be of interest and is written on the form

$$\mathbf{y} = \mathbf{g}(\mathbf{x}, \mathbf{u}) \tag{3.5}$$

where

$$\mathbf{y} = \begin{bmatrix} y_1 \\ y_2 \\ \vdots \\ y_m \end{bmatrix} \quad \mathbf{g} = \begin{bmatrix} g_1 \\ g_2 \\ \vdots \\ g_m \end{bmatrix} \tag{3.6}$$

y is the vector of outputs, and **g** is a vector of nonlinear functions relating state and input variables to output variables.

3.4 Linearization

Linearizing (3.5), and (3.6) about the operating point x_0 and u_0 yields the linearized state space system given by

$$\Delta\dot{\mathbf{x}} = \mathbf{A}\Delta\mathbf{x} + \mathbf{B}\Delta\mathbf{u} \tag{3.7}$$

$$\Delta\mathbf{y} = \mathbf{C}\Delta\mathbf{x} + \mathbf{D}\Delta\mathbf{u} \tag{3.8}$$

where

$$\mathbf{A} = \begin{bmatrix} \frac{\partial f_1}{\partial x_1} & \cdots & \frac{\partial f_1}{\partial x_n} \\ \cdots & \cdots & \cdots \\ \frac{\partial f_n}{\partial x_1} & \cdots & \frac{\partial f_n}{\partial x_n} \end{bmatrix} \quad \mathbf{B} = \begin{bmatrix} \frac{\partial f_1}{\partial u_1} & \cdots & \frac{\partial f_1}{\partial u_r} \\ \cdots & \cdots & \cdots \\ \frac{\partial f_n}{\partial u_1} & \cdots & \frac{\partial f_n}{\partial u_r} \end{bmatrix}$$

$$\mathbf{C} = \begin{bmatrix} \frac{\partial g_1}{\partial x_1} & \cdots & \frac{\partial g_1}{\partial x_n} \\ \cdots & \cdots & \cdots \\ \frac{\partial g_m}{\partial x_1} & \cdots & \frac{\partial f_m}{\partial x_n} \end{bmatrix} \quad \mathbf{D} = \begin{bmatrix} \frac{\partial g_1}{\partial u_1} & \cdots & \frac{\partial g_1}{\partial u_r} \\ \cdots & \cdots & \cdots \\ \frac{\partial f_m}{\partial u_1} & \cdots & \frac{\partial g_m}{\partial u_r} \end{bmatrix} \tag{3.10}$$

$\Delta\mathbf{x}$ is the state vector of dimension n, $\Delta\mathbf{y}$ is the output vector of dimension m, $\Delta\mathbf{u}$ is the input vector of dimension r, **A** is the state matrix of size $n \times n$, **B** is the input matrix of size $n \times r$, **C** is the output matrix of size $m \times n$ and **D** is the feedforward matrix which defines the proportion of input which appears directly in the output of size $m \times r$.

3.5 Eigenproperties of the state matrix

After the linearized state space of the power system is declared on the form given in (3.7) and (3.8), the stability can be assessed and investigated. The analysis performed follows standard root-locus methods found in most studies of inter-area oscillations. The eigenvalues of a matrix are given by the values of the scalar parameter λ for which there exist non-trivial solutions for the equation

$$\mathbf{A\Phi} = \lambda\mathbf{\Phi} \tag{3.11}$$

where $\mathbf{A}$ is the $n \times n$ matrix declared in the previous section and $\mathbf{\Phi}$ is an $n \times 1$ vector defined in Section 3.6.

Solving for λ (non-trivial solution) in (3.11) gives

$$det(\mathbf{A} - \lambda\mathbf{I}) = 0 \tag{3.12}$$

The eigenvalues $(\lambda_1, \lambda_2, \cdots, \lambda_n)$ are the the eigenvalues of the state matrix $\mathbf{A}$. The eigenvalues may be real or complex. If A is real, complex eigenvalues always occur in pairs.

The eigenvalues are on the form

$$\lambda = \sigma \pm j\omega \tag{3.13}$$

The operating point $(\delta_0,\ \omega_0)$ will be analyzed by studying the eigenvalues. If all eigenvalues are on the left-hand side of the imaginary axis, i.e., the real part σ, of (3.13) has a negative sign, the operating point is stable. Likewise, if some eigenvalue has a positive real part, the mode, as well as the system is unstable. The time dependent characteristics to an eigenvalue λ_i is given by $e^{\lambda_i t}$. Therefore, the real eigenvalue relates to a non-oscillatory mode. A negative real eigenvalue signifies a decaying mode. Larger magnitude means faster decay. A positive real eigenvalue signifies aperiodic instability. The complex pairs relate to an oscillatory mode. Condensing this information, an oscillatory mode containing a positive real part implies an unstable oscillatory mode. Likewise, an oscillatory mode containing a negative real part implies a stable oscillatory mode.

From eigenvalues, other information can be obtained. The frequency of oscillations is given by

$$f = \frac{\omega}{2\pi} \tag{3.14}$$

and the damping ratio which determines the rate of decay of the amplitude of the oscillation, which is given by

$$\zeta = \frac{-\sigma}{\sqrt{\sigma^2 + \omega^2}} \tag{3.15}$$

With the use of the proposed control solution in Section. 4, maximizing the damping ratio of the inter-area mode, while not decoupling the local modes of oscillation, is the goal of this thesis.

3.6 Eigenvectors

For any eigenvalue λ_i, the n-column vector which satisfies

$$\mathbf{A}\boldsymbol{\Phi}_i = \lambda_i \boldsymbol{\Phi}_i \tag{3.16}$$

is called the right eigenvector of A related to the eigenvalue λ_i. Similarity, the n-row vector Ψ_i which satisfies

$$\boldsymbol{\Psi}_i \boldsymbol{\Phi}_i = \lambda_i \boldsymbol{\Psi}_i \tag{3.17}$$

is called the left eigenvector of **A** related to the eigenvalue λ_i. Since the eigenvectors are determined only to within a scalar multiplier, it is common to normalize these vectors so

$$\boldsymbol{\Psi}_i \boldsymbol{\Phi}_i = 1 \tag{3.18}$$

3.7 Modal matrices

To express the eigenproperties of **A**, the following matrices are created

$$\boldsymbol{\Phi} = [\Phi_1 \quad \Phi_2 \quad \ldots \quad \Phi_n] \tag{3.19}$$

$$\boldsymbol{\Psi} = [\Psi_1 \quad \Psi_2 \quad \ldots \quad \Psi_n^T]^T \tag{3.20}$$

$\wedge = diagonal\ matrix, with\ the\ eigenvalues\ (\lambda_1, \lambda_2, \cdots, \lambda_n)$ as diagonal matrix

The relationships between (3.16), and (3.18) can be written in the compact form as

$$\mathbf{A}\boldsymbol{\Phi} = \boldsymbol{\Phi} \wedge \tag{3.21}$$

$$\boldsymbol{\Psi}\boldsymbol{\Phi} = 1 \quad \boldsymbol{\Psi} = \boldsymbol{\Phi}^{-1} \tag{3.22}$$

3.8 Participation factors

Using the right and left eigenvectors separately for identifying relationships between states, and modes cause problems as the eigenvectors are dependent on units and scaling associated with the state variables. In [21], combining the right and left eigenvector through a "participation matrix" was proposed, and is given by

$$\mathbf{P} = [p_1 \quad p_2 \quad \ldots \quad p_n] \tag{3.23}$$

with

$$p_i = \begin{bmatrix} p_{1i} \\ p_{2i} \\ \vdots \\ p_{ni} \end{bmatrix} = \begin{bmatrix} \Phi_{1i}\Psi_{i1} \\ \Phi_{2i}\Psi_{i2} \\ \vdots \\ \Phi_{ni}\Psi_{in} \end{bmatrix} \tag{3.24}$$

p_{ki} is the participation factor and is a measure of the relative participation of the kth state variable in the ith mode, and vice versa.

3.9 Mode shape

To eliminate cross-coupling between state variables, a new state vector z is declared related to the original state vector $\Delta\mathbf{x}$ by the transformation

$$\Delta\mathbf{x} = \mathbf{\Phi z} \tag{3.25}$$

The variables $x_1, x_2, \cdots, x_n$ are the original state variables chosen to represent the dynamic performance of the system. The variables $z_1, z_2, \cdots, z_n$ are the transformed state variables such that each variable is only associated with only one mode. This means that the transformed variables $\mathbf{z}$ are directly related to the modes.
The response of a particular state variable can be examined in each ith mode of the right eigenvector $\mathbf{\Phi}$. The response is called the mode shape of the individual oscillatory mode. E.g., the relative activity of the state variable of the state variable x_k in the ith mode is given by the element in Φ_{ki} of the right eigenvector Φ_i.

3.10 Controllability and observability

The state equations can now be written in the decoupled form though

$$\dot{\mathbf{z}} = \wedge\, \mathbf{z} + \mathbf{B}'\Delta\mathbf{u} \tag{3.26}$$

$$\Delta\mathbf{y} = \mathbf{C}'\mathbf{z} + \mathbf{D}\Delta\mathbf{u} \tag{3.27}$$

where

$$\mathbf{B}' = \mathbf{\Phi^{-1}B} \tag{3.28}$$

$$\mathbf{C}' = \mathbf{C\Phi} \tag{3.29}$$

The inputs of $\mathbf{B}'$ relates the inputs to the modes in the system. If the ith row of $\mathbf{B}'$ is zero, the inputs have no impact on the ith mode. In this case, the ith mode is said to be uncontrollable. $\mathbf{B}'$ is therefore called the mode controllability matrix. In other words, a full row rank means the mode is controllable.

The inputs of $\mathbf{C}'$ relates the state variables $\mathbf{z_i}$ to the outputs of the system. If the column is zero, the corresponding mode is unobservable. $\mathbf{C}'$ is therefore called the mode observability matrix. In other words, a full column rank means the mode is observable.

3.11 Residues

The residue provides an idea of how a particular mode is affected by the input and how visible is from the output, i.e., the residues are clear measures of joint controllability and observability of a particular oscillation mode. The residues for the ith mode are given by

$$R_i = \mathbf{C\Phi_i\Psi_i B} \tag{3.30}$$

3.12 Hankel singular value

The solution P and Q of the system of (3.31) and (3.32) are called controllability and observability gramian respectively

$$\mathrm{P}\mathbf{A}^{\mathrm{T}} + \mathbf{A}\mathrm{P} + \mathbf{B}\mathbf{B}^{\mathrm{T}} = 0 \tag{3.31}$$

$$Q\mathbf{A} + \mathbf{A}^T Q + \boldsymbol{C}^T \boldsymbol{C} = 0 \tag{3.32}$$

The singular value of the product of controllability and observability gramian is given by

$$\varrho(PQ) = \Sigma = diag[\varrho_1, \varrho_2, \ldots, \varrho_n] \tag{3.33}$$

The ϱ_i is called Hankel singular values of the system, ordered as $\varrho_1 \geq \varrho_2 \geq \ldots \geq \varrho_n > 0$. The Hankel singular value can be written as

$$\varrho_i = \lambda_i \sqrt{PQ} \tag{3.34}$$

For choosing input and output signals, the Hankel singular values can be calculated for each combination of input and output. The candidate with the largest Hankel singular values shows the best controllability and observability properties [9].

3.13 Summary

After the oscillatory modes are known and the modal matrices declared, analysis is performed to identify specific rotor-angle modes. These modes provide the largest contribution to the low frequency oscillations. Analyzing the right and left eigenvectors in combination with the participation factors can be used to identify these modes. Then, the mode shape of the rotor-angle modes is studied to identify if it is local or inter-area type. Once the modes have been identified, the observability and controllability indices can be calculated. An example is presented in Section. 6.1 for clarity. Examples were residues and Hankel singular are used is given in Section. 6.2 and 6.3. The methodology that will be used for the proposed control strategy in Section. 4, and can be summarized as:

i. Build the test system of choice, in this case, the two area, four machine system, **excluding the FACTS device and POD.**
ii. Acquire the state-space model of the system. For PSAT, the system can be acquired by executing the command "fm_abcd" in Matlab.
iii. Identify the oscillatory modes by finding the eigenvalues of the **A**-matrix. The oscillatory modes will include a complex conjugate pair.
iv. To identify the rotor-angle modes, participation factors must be studied. The modes where the rotor angle state variables are the most associated states will be the rotor angle modes.
v. To identify which modes are local and inter-area modes, the mode shape, i.e., the right eigenvector entries must be studied. E.g., for local area 1, the angle between generator 1 and 2s right eigenvector entry will be approximately 180 degrees as they are swinging against each other, with an amplitude in the same range.
vi. Study the absolute value of the residues for the systems inter-area mode to find which bus/line provides the highest joint controllability and observability, then place the FACTS device on this location.
vii. Repeat step i.-v. except the instruction marked with bold font in Step. i..
viii. Perform Hankel singular value analysis on the inter-area mode for each combination of input signal and location, then choose the combination offering the greatest value. If the greatest value appears on the local bus of the FACTS → no need for PMU.
ix. Tune the POD with the residue phase compensation method described in Section. 4.4.
x. Verify the design through simulations. The expected result is an improvement of the inter-area mode damping ratio, while not impairing the damping ratio of the local modes with respect to the initial test system. Other unstable modes should not appear.

4 Proposed control strategy

The broad topic of power oscillation dampers includes methodologies of combining the POD with different FACTS devices, the study of different controller designs, and review of different tuning methods. The investigation of modifying of the input signal for a specific power oscillation damper applied to a FACTS device installed in a power system is the main objective of this thesis and is not aimed to serve as a comprehensive study of the field of POD design and application. However, an assessment of a few controller designs, tuning methodologies and input signals will be outlined in this chapter with the purpose of damping inter-area oscillations.

4.1 Choice of FACTS device

Since the purpose of this thesis is to show improved damping, controlling the FACTS-device through a POD, the FACTS-device itself should not provide significant quantities of damping. Due to losses, transmission system operators prefer the installment of shunt FACTS devices over series FACTS devices [1]. It is preferable that the device can deliver good voltage support via reactive power generation. In [31,32] the SVCs where found fulfil these criterions. The mathematical model of the particular SVC used is found in Section. 5.5.

4.2 Controller design

Figure.17 displays a lead-lag controller used for the POD in this thesis. Other controllers do exist like the proportional-integral-derivative controller proposed in [10], and more advanced artificial intelligence controllers like the fuzzy-controlled POD in [11]. With each controller having its own respective assets and liabilities, their performance seems approximately inseparable. The purpose of this thesis in not to make a comprehensive comparison of different control strategies for the POD, but rather display the improvement regarding damping by including global signals from PMU. The first block of the controller structure is the gain K which is of great importance. The stability increases proportional with the increase of this value, up to a certain point. The gain represents how sensitive the controller is to change in the input signal. The second block is the washout block which lowers over-sensitive response of during the time-period of severe faults like short circuits or sudden load changes. The washout block acts as a high pass filter which passes the frequencies of interest. For the lead-lag block, the time constants T_1 and T_2 are chosen from the requirements of the phase compensation to achieve damping torque. This is since the POD strive to produce an electrical torque in phase with the speed deviation, therefore, phase lead block circuits are used to compensate for the lag between its output and control action, i.e., electrical torque [1]. The number of lead-lag blocks can vary but is usually two. Some lead-lag structures include an additional block with the time constants T_3 and T_4 in the second lead-lag block. For this thesis, two lead-lag blocks will be used, meaning $m = 2$. The transfer function derived from the figure below is given by

$$H_{POD} = K\frac{sT_W}{1+sT_W}\left(\frac{1+sT_1}{1+sT_2}\right)^m \tag{4.1}$$

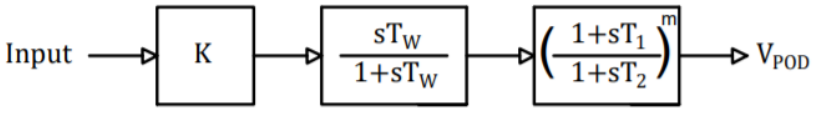

Figure. 17. Block diagram for a lead-lag POD

4.3 Input signals

The usual input signals for POD include line current, real power, reactive power, and bus voltage. In this thesis, an analysis will be performed to determine which of the before-mentioned input signals provides the most information regarding this particular system.

Since the structure and purpose of the POD is like that of a PSS, and PMU realize the opportunity of providing remote signals, typical PSS input signals may be considered for POD. Unlike the POD, PSSs usually utilize rotor speed deviations as input. Some PSSs used voltage or power as an input like that of the POD. Frequency has been tested as an input but was found highly sensitive to the stiffness of the transmission system, i.e., more sensitive when the stiffness is reduced. This means that the signal is more sensitive to inter-area oscillations, which for PSSs reduced local stability [1]. This might be beneficial for a POD installed on tie-lines. The drawback of this input signal was the introduction of sudden phase shifts after severe faults and signal noise from industrial loads.

4.4 Tuning

Differing criterions of local and inter-area oscillation damping and stability during small-signal and transient stability circumstances have produced a vast majority of tuning techniques for PODs. Tuning techniques investigated all designed for lead-lag controller tuning is the residue phase compensation [1] ,[13], pole placement also called decentralized modal control [14], eigenvalue technique [15], tuning based on frequency response [16], sparsity technique [17], and more recent control strategies using artificial intelligence like the genetic algorithm [18], and differential evolution grey wolf optimization algorithm found in [19]. With each tuning method having its own respective assets and liabilities, large performance differs with different tuning techniques applied for this test system seems unlikely. The purpose of this thesis in not to make a comprehensive comparison of different tuning techniques for the POD, but rather display the improvement on damping by including global signals from PMU. The tuning used in this thesis is the residue phase compensation technique. The washout time constant should be in the range of 10-20 s for the purpose of damping inter area oscillations [13]. Recalling from Section. 3.11, the residue R_i is the residue with regards to the ith mode, the amount of phase required compensation ϕ_i, regarding the ith mode, is given by

$$\phi_i = \pi - arg R_i \tag{4.2}$$

where arg means the angle in radians of the respective residue expressed in phasor form.

With f_i being the frequency of the ith mode, the lead-lag parameters are given by

$$\psi = \frac{T_1}{T_2} = \frac{1 - sin\frac{\phi_i}{m}}{1 + sin\frac{\phi_i}{m}} \tag{4.3}$$

$$T_1 = \frac{1}{2\pi f_i \sqrt{\psi}} \tag{4.4}$$

$$T_2 = \psi T_1 \tag{4.5}$$

4.5 Time-delay associated with remote signals

Varying time-delay introduced by communication networks when transferring remote signals from PMUs may degrade performance and cause instability for excessive time delays [20]. The time delay may vary from tens to hundreds of milliseconds, depending on the type of communication system, conditions, distance, etcetera. Literature addressing the topic of time delays is already in place. In [21], a decentralized load modulation system was developed where non-linear bang-bang action was used to deal with time-delay for a PMU. In [22], a delay estimator based on a unified smith predictor approach using linear matrix inequalities and pole-placement constraints was developed for remote signals used in a damping controller for a prototype power system.

For this thesis, it is assumed an ideal measurement, meaning infinite sampling rate leading to an actual representation of the measured phasor, and without the presence of time-delay.

5 Mathematical modelling

The following section presents the mathematical models used for the generator, excitation systems, power system stabilizers as well as the FACTS-device. The models are created in Power System Analyzing Toolbox (PSAT), a toolbox for Matlab.

5.1 Synchronous generator

PSAT models its sixth-order generator with various simplifications using the Park-Concordia model [37]. A clear description of a similar model is given in [26]. The precision of this generator model is deemed sufficient for this study. Higher detailed sixth-order models, like the linearization of the model described in Appendix B is found in [1].

The link between network phasors and machine voltage is

$$v_d = Vsin(\delta - \theta) \tag{5.1}$$

$$v_q = Vcos(\delta - \theta) \tag{5.2}$$

The machines have six algebraic equations with two being the real and reactive power injections at the network buses, and the others being

$$0 = e_d i_d + e_q i_q - P \tag{5.3}$$

$$0 = e_q i_d + e_d i_q - Q \tag{5.4}$$

$$0 = p_{m0} - p_m \tag{5.5}$$

$$0 = e_{fd0} - e_{fd} \tag{5.6}$$

where p_m and e_{fd} are the mechanical power and field voltage algebraic equations. The field voltage includes a feedback of the rotor speed and the active power produced

$$e_{fd}^* = e_{fd} + K_\omega(\omega - 1) - K_p(P(\mathbf{x}, V, \theta) - P_0) \tag{5.7}$$

where **x** are the state variables.

The state-space form of the generator consists of the time-derivative of the four flux terms, and the change in rotor speed and angle

$$\frac{d\delta}{dt} = \dot{\delta} = \omega_0 \Delta\omega_r \tag{5.8}$$

$$\frac{d\omega_r}{dt} = \dot{\omega_r} = \frac{1}{2H}(T_m - T_e - K_D \Delta\omega_r) \tag{5.9}$$

These two equations represent the operating point in which the system is linearized around, i.e., the $\dot{x} = f(x, u)$ model of the system. The remaining state equations are given by

$$\dot{e}'_q = \frac{-f_s {e'}_q - \left(x_d - {x'}_d - \frac{{\tau''}_{d0}{x''}_d}{{\tau'}_{d0}{x'}_d}(x_d - {x'}_d){i}_d + \left(1 - \frac{\tau_{AA}}{{\tau'}_{d0}}\right) e *_{fd}\right)}{{\tau'}_{d0}} \tag{5.10}$$

$$\dot{e}_q'' = \frac{-e''_q + e'_q - \left(x'_d - x''_d - \frac{\tau''_{d0} x''_d}{\tau'_{d0} x'_d}(x_d - x'_d) i_d + \left(1 - \frac{\tau_{AA}}{\tau'_{d0}}\right) e *_{fd}\right)}{\tau''_{d0}} \quad (5.11)$$

$$\dot{e}_d' = \frac{-e_d + \left(x_q - x'_q - \frac{\tau''_{q0} x''_q}{\tau'_{q0} x'_q}(x_q - x'_q) i_q\right)}{\tau'_{d0}} \quad (5.12)$$

$$\dot{e}_d'' = \frac{-e''_d + e'_d + \left(x'_q - x''_q - \frac{\tau''_{q0} x''_q}{\tau'_{q0} x'_q}(x_q - x'_q) i_q\right)}{\tau''_{d0}} \quad (5.13)$$

where τ_{AA} is the d-axis additional leakage time constant.

5.2 Automatic Voltage Regulator

The excitation system is a simple high gain thyristor exciter and is displayed in Figure. 18. Its linearized state equations are given below. Its parameters are explained in Table. I [37].

$$\dot{v}_m = \frac{E_t - v_m}{T_r} \tag{5.14}$$

$$\dot{v}_r = \begin{cases} v_r * \longrightarrow v_{rMIN} \leq v_r * \leq v_{rMAX} \\ v_{rMAX} \longrightarrow v_r * > v_{rMAX} \\ v_{rMIN} \longrightarrow v_r * < v_{rMIN} \end{cases} \tag{5.15}$$

$$\dot{E}_{fd} = \frac{-(E_{fd} - v_r)}{T_{fd}} \tag{5.16}$$

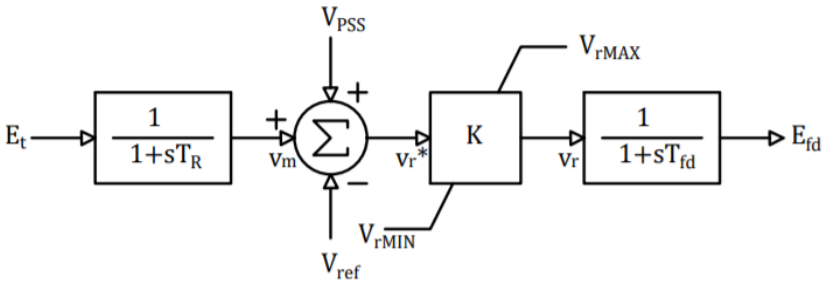

Figure. 18. AVR block diagram.

Table. I
AVR parameter description

Name	Unit	Description
T_{fd}	Seconds	Field circuit time constant
T_R	Seconds	Regulator time constant
K	pu	Voltage regulator gain
V_{rMAX}	pu	Maximum voltage regulator output
V_{rMIN}	pu	Minimum voltage regulator output

5.3 Power System Stabilizer

The PSS used is of the type lead-lag and is displayed in Figure. 19. Its linearized state equations are given below. Its parameters are explained in Table. II [37].

$$\dot{v}_1 = \frac{-(Kv_I + v_1)}{T_W} \tag{5.17}$$

$$\dot{v}_2 = \frac{\left(1 - \frac{T_1}{T_2}\right)\left(v_2 + \frac{T_1}{T_2}(Kv_I + v_1)\right) - v_2}{T_2} \tag{5.18}$$

$$\dot{v}_{PSS} = \frac{\left(1 - \frac{T_3}{T_4}\right)\left(v_2 + \frac{T_1}{T_2}(Kv_I + v_1)\right) - v_{PSS}}{T_4} \tag{5.19}$$

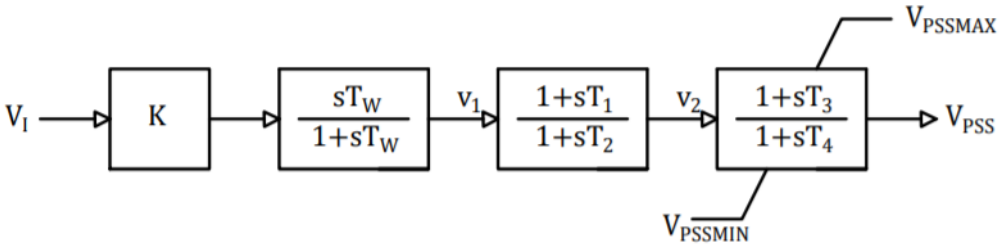

Figure. 19. PSS block diagram

Table. II
PSS parameter description

Name	Unit	Description
K	pu	Stabilizing gain
T_W	Seconds	Washout time constant
T_1	Seconds	Lead-lag time constant
T_2	Seconds	Lead-lag time constant
T_3	Seconds	Lead-lag time constant
T_4	Seconds	Lead-lag time constant
V_{PSSMAX}	pu	Maximum stabilizing voltage output
V_{PSSMIN}	pu	Minimum stabilizing voltage output

5.4 Power Oscillation Damper

The POD used is of the type lead-lag and is displayed in Figure. 20. Its linearized state equations are given below. Its parameters are explained in Table. III [37]. For the exact representation of the POD proposed in Section. 4.2, $T_1 = T_3$ and $T_2 = T_4$.

$$\dot{v}_1 = \frac{-(K\ Input_{PMU} + v_1)}{T_W} \tag{5.20}$$

$$\dot{v}_2 = \frac{\left(1 - \frac{T_1}{T_2}\right)\left(v_2 + \frac{T_1}{T_2}(K\ Input_{PMU} + v_1)\right) - v_2}{T_2} \tag{5.21}$$

$$\dot{v}_{POD} = \frac{\left(1 - \frac{T_3}{T_4}\right)\left(v_2 + \frac{T_1}{T_2}(K\ Input_{PMU} + v_1)\right) - v_{POD}}{T_4} \tag{5.22}$$

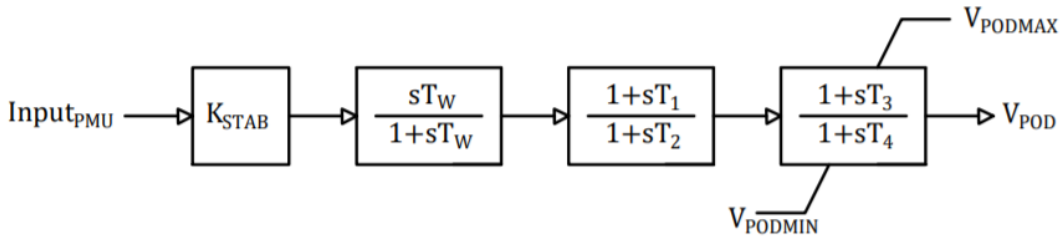

Figure. 20. POD block diagram.

Table. III
POD parameter description

Name	Unit	Description
K	pu	Stabilizing gain
T_W	Seconds	Washout time constant
T_1	Seconds	Lead-lag time constant
T_2	Seconds	Lead-lag time constant
T_3	Seconds	Lead-lag time constant
T_4	Seconds	Lead-lag time constant
V_{PODMAX}	pu	Maximum stabilizing voltage output
V_{PODMIN}	pu	Minimum stabilizing voltage output

5.5 Static VAR Compensator

The SVC used in the study considers the susceptance b, and is displayed in Figure. 21. Its linearized state equation is given below. Its parameters are explained in Table. IV [37].

$$\dot{b}_{SVC} = \frac{K\left(V_{ref} + V_{POD} - V_I\right) - b_{SVC}}{T_R} \tag{5.2}$$

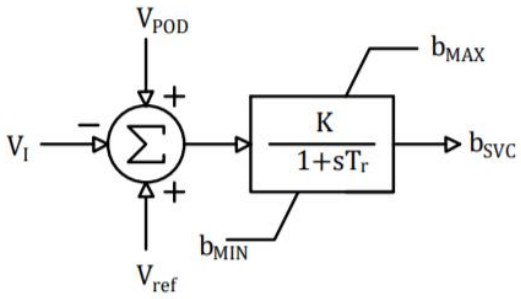

Figure. 21. SVC block diagram.

Table. IV
SVC parameter description

Name	Unit	Description
T_R	Seconds	Regulator time constant
K	pu	Regulator gain
b_{MAX}	pu	Maximum susceptance
b_{MIN}	pu	Minimum susceptance

6 Simulating results

Program

Power System Analyzing Toolbox was used in conjunction with MATLAB to perform the small-signal and transient stability analysis via time-domain simulations. Briefly, this program calculates the load flow based on the topological data of the power system, then utilizes the parameters of the machines and controls in the system combined with the load flow results to perform time-domain simulations. The toolbox allows for extracting the state-space model, necessary for the small-signal stability analysis describes in Section. 3.

Test system

Inter-area oscillations in large interconnected systems are complex. There are generally many such modes, each involving numerous generators. The complexity of the system models necessary to determine the stability of specific power systems, obscures the fundamental nature of inter-area modes. Therefore, to be able to concentrate on those factors which affect inter-area modes, the two-area, four-machine system, shown in Figure. 22 was developed, which includes both inter-area and local modes. Although small, the system parameters, and structure are realistic. The system is particularly useful for parametric studies. The base system is symmetric; it consists of two identical areas connected through a relatively weak tie. Each area includes two generating units with equal power outputs. The full symmetry of the base system clarifies the effect that various factors have on the inter-area mode. The test system is often used as a reference for the before-mentioned problem [1,30].

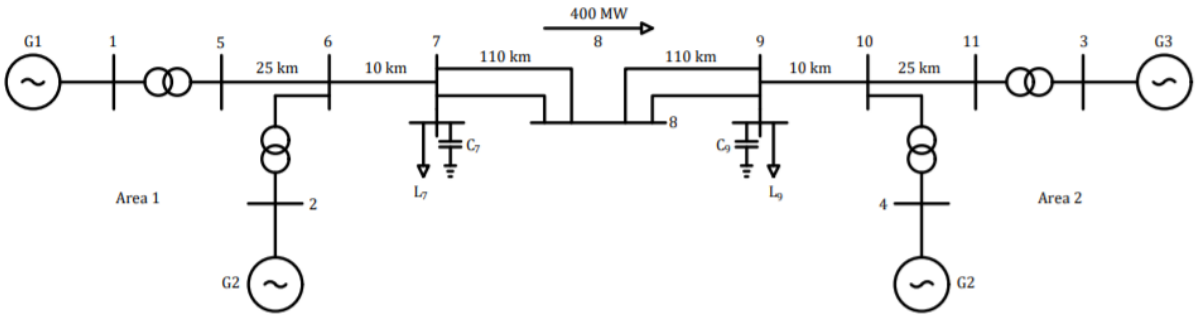

Figure. 22. Line diagram of the two-area, four-machine system.

Each area consists of two coupled units, each having a rating of 900 MVA and 20 kV. The per unit parameters of the generators on the rated MVA and kV base are given in Table. V.

Each generator is equipped with an AVR with the parameters given in Table. VI.

Each AVR is equipped with a PSS whose input is $\Delta\omega = P_m - P_e$ with the parameters given in Table. VII.

Each of the step-up transformers has an impedance of 0+j0.15 per unit on 900 MVA and 20/230 kV base. The off-nominal tap ratio is 1.0.

The transmission system nominal voltage is 230 kV and the per unit parameters of the lines on 100 MVA, 230 kV base are given by

$$R_\ell = 0.0001\ pu/km, X_\ell = 0.001\ pu/km, b_C = 0.00175\ pu/km$$

where b_C is the capacitive susceptance of the line.

Area 1 is exporting 400 MW to area 2, and the loading of the generating units are given in Table. VIII.

The loads and reactive power supplied by the shunt capacitors at bus 7 and 9 is given in Table. IX.

Table. VI
Generator parameters

Parameter	Value
X_d	1.8
X_q	1.7
X'_d	0.3
X'_q	0.55
X''_d	0.25
X''_q	0.25
R_a	0.0025
X_l	0.2
T'_{d0}	8.0 s
T'_{q0}	0.4 s
T''_{d0}	0.03 s
T''_{q0}	0.05 s
A_{Sat}	0.015
B_{Sat}	9.6
K_d	0
H	6.5 $(G1, G2)$ 6.175 $(G3, G4)$

Table. VI
AVR parameters

Name	Unit
T_{fd}	0.001 s
T_R	0.01 s
K	200.0 pu
V_{rMAX}	10.0 pu
V_{rMIN}	-10.0 pu

Table. VII
PSS parameters

Name	Unit
K	20.0 pu
T_W	10.0 s
T_1	0.05 s
T_2	0.02 s
T_3	3.0 s
T_4	5.4 s
V_{PODMAX}	0.2 pu
V_{PODMIN}	-0.2 pu

Table. VIII
Generator loading

Generator	Active power [MW]	Reactive power [MVAR]	Voltage [pu]
G1	700	185	$1.03\angle 20.2°$
$G2$	700	235	$1.01\angle 10.5°$
$G3$	719	176	$1.03\angle -6.8°$
$G4$	700	202	$1.01\angle -17.0°$

Table. IX
Load data

Bus	Active power [MW]	Reactive power [MVAR]	Reactive power supplied [MVAR]
7	967	100	200
9	1767	100	350

6.1 Example: small-signal stability with no supplementary control

To further establish understanding from Section. 3, and how the impacts of the subsequent control strategies are studied, the test system will first be studied without any supplementary control. As displayed in Section. 5.1, each generator contains six state variables. The **A**-matrix of the system therefore becomes 24x24 since there are 4 generators.

The oscillatory profile of the systems is gathered from the eigenanalysis. The eigenvalues containing complex conjugates represents oscillatory modes. The frequency and damping factors of each oscillatory mode can be calculated, and inter-area and local-area modes are identified by studying the magnitude of the participation factor of each oscillatory mode with respect to the rotor angle δ. Studying the right eigenvector entries for each rotor angle modes gives the mode shape which determines if the particular modes are local area or inter-area modes.

Table. X contains information about the three rotor angle modes. Table. XI, XII and XIII contains the participation factors of the three oscillatory modes. Table. XIV contains its right eigenvector entries, with Figure. 23 displaying them in the complex plane.

Table. X
Oscillation profile for test system w/o supplementary control.

Area	Eigenvalues	Frequency [Hz]	Damping ratio
Local 1	-0.50836±6.0017i	0.95519	0.0844
Local 2	-0.51722±6.1779i	0.98324	0.0834
Inter	-0.12792±3.1397i	0.49969	0.0407

Table. XI
Local area 1 participation factors

Generator	$\dot{\delta}$	$\dot{\omega}$	$\dot{e}'_q$	$\dot{e}''_q$	$\dot{e}'_d$	$\dot{e}''_d$
1	**0.19599**	**0.19599**	0.01019	0.00361	0.01225	0.00571
2	**0.25005**	**0.25005**	0.00861	0.00305	0.0267	0.01245
3	0.00855	0.00855	0.00047	0.00017	0.0004	0.00019
4	0.00318	0.00318	0.00005	0.00003	0.00039	0.00018

Table. XII
Local area 2 participation factors

Generator	$\dot{\delta}$	$\dot{\omega}$	$\dot{e}'_q$	$\dot{e}''_q$	$\dot{e}'_d$	$\dot{e}''_d$
1	0.00401	0.00401	0.0001	0.00004	0.00057	0.00027
2	0.00675	0.00675	0.00047	0.00018	0.00031	0.00015
3	**0.19095**	**0.19095**	0.01041	0.00388	0.00984	0.00474
4	**0.25643**	**0.25643**	0.00841	0.00314	0.02782	0.01339

Table. XIII
Inter-area participation factors

Generator	$\dot{\delta}$	$\dot{\omega}$	$\dot{e}'_q$	$\dot{e}''_q$	$\dot{e}'_d$	$\dot{e}''_d$
1	**0.09039**	**0.09039**	0.01134	0.00145	0.00123	0.00033
2	**0.04979**	**0.04979**	0.01195	0.00153	0.0033	0.00089
3	**0.19084**	**0.19084**	0.00602	0.00077	0.00083	0.00023
4	**0.14516**	**0.14516**	0.0045	0.00057	0.00213	0.00058

Table. XIV
Right eigenvector entries for the three oscillatory modes

Area	Generator	Mode shape (right eigenvector entry)
Local 1	G1	-2.5746-0.0288i
	G2	0.6772+0.0000i
Local 2	G3	-0.5661-0.0287i
	G4	0.7011+0.0000i
Inter	G1	0.2909+0.0826i
	G2	0.2069+0.0816i
	G3	-0.6649+0.0000i
	G4	-0.6156+0.00134i

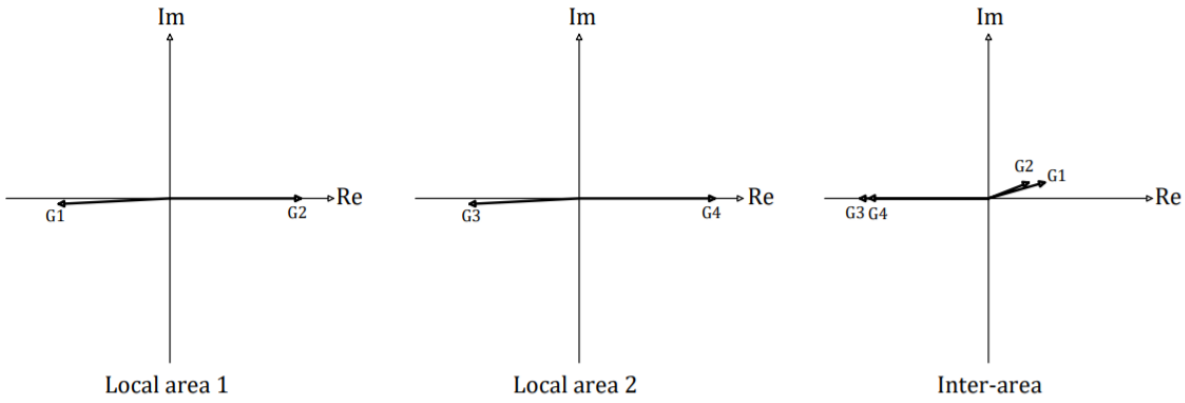

Figure. 23. Visual representation of the mode shapes of three oscillatory modes.

Self-explanatory, the rotational speed ω and the rotor angle δ has the largest magnitude of participation in the rotor angle modes confirming that these modes are indeed rotor angle modes. Worth noting, is the similar values of participation for these two state variables. Once additional control strategies where introduced (AVR, PSS, etc.), a numerical difference occurs between the magnitude of the two before-mentioned state variables.

For the local area modes, the generators in the opposing area have significantly lower magnitude of participation than the generators involved in the particular area. In this case the generators involved in area 2 has a greater rotor angle participation than those of area 1. All modes of oscillation are stable, hence the negative sign of the real part in Table. X.

Studying the right eigenvector entries makes the identification of local and inter-area modes possible. For the local modes, the generators swing incoherently, hence the opposite sign of the right eigenvector entries. The inter-area mode is identified where the right eigenvector entries of the generators in one particular area has the opposite sign as the generators in the other area. This indicates the generators of one area is swinging against the generators in the other area as seen in Figure. 23. The greater participation factors of generators 3 and 4 with respect to 1 and 2 can also be seen in the amplitude of their mode shapes.

6.2 Small signal stability with FACTS

Before approaching this section, readers not comprehensively familiar with PSAT is referred to "Appendix A" detailing information regarding the structure of **C**-matrices in PSAT.

The AVR modelled in Section. 5.2, PSS from Section. 5.3, and the SVC from Section. 5.5 is now added with respect to the system in Section. 6.1. Its tuning parameters are given in Table. XV.

Table XV
SVC tuning parameters

Name	Unit
T_r	0.05 s
K	50.00 pu
V_{ref}	1.011 pu
B_{MAX}	2.00 pu
B_{MIN}	-1.00 pu

With each generator having six state variables, each AVR having three, each PSS having three, and the SVC having one, the state space matrix is of the dimension 49x49. Again, each mode of interest is identified studying eigenvalues containing complex conjugates, participation factors, and right eigenvector entries.

To find optimal placement of the SVC, the normalized form of the residue method described in Section. 3.11 is used, i.e., the largest absolute value of the of the complex number for the residue value is set as reference at 1.0000. The calculated residue for the SVC is given in Table. XVI. Section. 5.5 showed that the input for the SVC was voltage. Since the SVC uses voltage as input, the **C**-matrix was based on receiving end voltage of the lines.

Table XVI
Normalized form of the absolute value of residue

Bus	Residue
6	0.0852
7	0.8498
8	**1.0000**
9	0.3462
10	0.0958

The result from the residue method is as expected. Since FACTS-devices are installed to improve voltage profile by regulating reactive power, it should generally be installed at the bus closest to the load center, which often has low voltage levels [1]. The residue method confirmed this theory with Bus 8 having the highest residue. For practical applications this is convenient as FACTS-devices are large and bulky.

The oscillation profiles for the test system including AVR, AVR+PSS, and AVR+PSS+SVC are showcased in Table. XVII.

Table. XVII
Oscillation profile for the test cases

AVR [36x36]	Eigenvalue	Frequency [Hz]	Damping ratio
Local area 1	-0.74072±6.1912i	0.985	0.11879
Local area 2	-0.74373±6.3880i	1.017	0.11564
Inter-area	+0.01920±3.5007i	0.557	-0.00548
AVR+PSS [48x48]	Eigenvalue	Frequency [Hz]	Damping ratio
Local area 1	-2.76100±7.4351i	1.183	0.34811
Local area 2	-2.88600±7.9044i	1.258	0.34297
Inter-area	-0.54464±3.4756i	0.553	0.15481
AVR+PSS+SVC [49x49]	Eigenvalue	Frequency [Hz]	Damping ratio
Local area 1	-2.79101±7.7195i	1.229	0.34001
Local area 2	-2.88321±8.2494i	1.313	0.32993
Inter-area	-0.59671±3.7195i	0.592	0.15840

Adding an AVR to each generator introduced negative damping with respect to the system in Section. 6.1, for the reasons discussed in Section. 2.3.3, leaving an unstable system. Adding a PSS to each AVR drastically improved the damping ratio of both local- and inter-area modes via the mechanism discussed in Section. 2.3.4. The small improvements in damping with respect to the inter-area mode was seen when adding the SVC for the reason discussed in Section. 2.3.5. Section. 4.1 stated that the SVC does not provide much damping torque itself, and simulations showed the device only improved the damping slightly over 2%. For improving its damping torque, it necessary to complement the SVC with a properly tuned POD. Implementing the SVC caused a slight decrease in damping ratio of the local modes, although small enough to categorize as insignificant.

6.3 Small signal stability with FACTS + local feedback POD

The test system is the same as that of Section. 6.2, however the POD from Section. 5.4 is now added, giving a state space matrix of the dimension 52x52. The PODs input comes from BUS 8, hence local feedback. Input candidates for the POD include line current, real power, reactive power, and bus voltage. A Hankel Singular Value analysis was performed on the state space system like that performed in [9]. This was done by expressing the C-matrix of the state space model based on current, real power, reactive power, and voltage. The bus voltage offered the largest magnitude of Hankel singular values, followed by real power, then current, and lastly, reactive power. This means the voltage contains more information about the systems internal states compared to other signal candidates. A summary of the normalized Hankel singular values is displayed in Table. XVIII, meaning the value of greatest magnitude obtains the value of 1.000.

Table. XVIII
Normalized Hankel singular value contribution of different input signals

Input signal	Hankel singular value
Current	0.4418
Real power	0.4435
Reactive power	0.2576
Voltage	**1.000**

The value of residue gathered from the modal analysis of the inter-area mode is 0.0083+0.3946i which from Section. 4.4 gives the parameters given in Table. XIX.

Table. XIX
POD tuning parameters

Name	Unit
T_W	10 s
T_1	0.6588 s
T_2	0.1097 s
V_{PODMAX}	0.2 pu
V_{PODMIN}	-0.2 pu

Once the parameters of the lead-lag compensation part of the POD is calculated, the gain *K* can be adjusted to obtain the most desired response from the controller. This is done by varying its value over a wide-ranging area, and studying the eigenvalue of the mode of interest, i.e., the inter-area mode. The summary of the local feedback gain adjustment is shown in Table. XX.

Table. XX
Summary of gain adjustment

Gain	Eigenvalue	Damping ratio
0.1	-0.60791±3.6831i	0.16295
0.2	-0.62418±3.6873i	0.16690
0.3	-0.63440±3.6982i	0.16907
0.4	**-0.63762±3.7094i**	**0.16941**
0.5	-0.63689±3.7180i	0.16883
0.6	-0.63470±3.7240i	0.16801
0.7	-0.63223±3.7281i	0.16719
1.0	-0.62605±3.7343i	0.16534
1.5	-0.62011±3.7377i	0.16367
2.0	-0.61695±3.7389i	0.16280
3.0	-0.61373±3.7396i	0.16195
5.0	-0.61117±3.7400i	0.16128
10.0	-0.60928±3.7401i	0.16079
20.0	-0.60834±3.7401i	0.16054

The adjustment of gain provided a modest performance increase with the gain of 0.4 increasing the damping ratio to a maximum value of 0.16941. Finer adjustments were made in the gain interval of $0.30 < K < 0.50$, with insignificant improvement in damping ratio. Further increase of gain drives the real part of the eigenvalue closer to the imaginary axis until the gain of $K = 0.43$, and cause an increase in the frequency of oscillation until the gain of $K = 10.0$, hence, the increased magnitude of the imaginary part of the eigenvalue.
Including the local feedback POD enhances the damping ratio of almost 7% compared to that of the SVC without supplementary control. A slight reduction of damping ratio is observed in the local areas, though insignificant and will not be further discussed in this section. The complete oscillation profile is given in Table. XXI.

Table. XXI
Oscillation profile for local feedback POD

AVR+PSS+SVC+local feedback POD [52x52]	Eigenvalue	Frequency [Hz]	Damping ratio
Local area 1	-2.7907±7.7385i	1.232	0.33924
Local area 2	-2.8852±8.2802i	1.318	0.32904
Inter-area	-0.63762±3.7094i	0.590	0.16941

6.4 Small signal stability with FACTS + remote feedback POD

The test system is the same as that of Section. 6.3, however the POD now utilizes remote signals from the PMU. The state space matrix is still of the dimension 52x52. To find the optimal location the PMU providing input signal for the POD, the Hankel singular values is again studied, with every input combination for every bus/line. The voltage of Bus 11 showed the greatest magnitude of Hankel singular values. This is the bus closest to generator 3 (after the step-up transformer), which its rotor angle is the most associated state in the inter-area mode. Since this is not the local bus of the FACTS-device, a PMU is needed. The normalized values are given in Table. XXII. As the phase compensation tuning method is based on the residues for the system excluding the POD, the parameters for the POD are the same as that in Table. XIX, however the tuning method suggests a new gain adjustment as the location of input signal is changed. The summary of the remote feedback gain adjustment is shown in Table. XXIII.

Table XXII
Hankel singular values for voltage input

Bus	Hankel singular value
5	0.5785
6	0.4194
7	0.3107
8	0.2774
9	0.2384
10	0.4113
11	**1.000**

Table XXIII
Summary of gain adjustment

Gain	Eigenvalue	Damping ratio
0.1	-0.60337±3.6996i	0.16107
0.5	-0.63776±3.6578i	0.17176
1.0	-0.69395±3.6114i	0.18870
2.0	-0.84791±3.5638i	0.23146
3.0	-1.0023±3.6130i	0.26732
4.0	**-1.0847±3.7130i**	**0.28041**
5.0	-1.1106±3.8018i	0.28040
6.0	-1.1114±3.8678i	0.27617
7.0	-1.1029±3.9158i	0.27111
10.0	-1.0683±3.9978i	0.25816

The adjustment of gain provided a performance increase with the gain of 4.0 increasing the damping ratio to a maximum value of 0.28041. Finer adjustments were made in the gain interval of $3.0 < K < 5.0$, with insignificant improvement in damping ratio. Further increase of gain drives the real part of the eigenvalue closer to the imaginary axis until the gain of $K = 6.2$, however the increased frequency of oscillation impedes the growth of the damping factor. The increase of frequency as a function of increased gain can be seen when increasing the gain beyond 2.0. A high gain usually precipitates instability as the controller may become too sensitive. At $K = 10.0$, an unstable mode appears suggesting an unstable system [1], however, this is not an oscillatory mode.

Including the global feedback POD enhances the damping ratio by almost 67% compared to that of the POD with local feedback control. The results are as expected as the Hankel singular value of the voltage of Bus 11 was much greater than that of the local signals at Bus 8, suggesting the input signal contains more information about the internal states of the system [9]. The summation of the participation factors of the three state variables for the POD

with respect to the inter-area mode increased from 0.01471 to 0.05056 when including the global signals, indicating an increase in observability and/or controllability of the POD for the inter-area mode, compared to that of the local input POD.
The complete oscillation profile is given in Table. XXIV. A slight increase in damping ratio is observed in the local areas, though insignificant and will not be further discussed in this section.

Table XXIV
Oscillation profile for the global input POD

AVR+PSS+SVC+global feedback POD [52x52]	Eigenvalue	Frequency [Hz]	Damping ratio
Local area 1	-2.8279±7.8279i	1.246	0.33977
Local area 2	-3.0211±8.4202i	1.311	0.33771
Inter-area	-1.0847±3.7130i	0.5909	0.28041

6.5 Robustness assessment 1: small-signal stability

To investigate robustness of the proposed controller for small signal-stability, the damping ratio of the inter-area mode was investigated over a broad range of tie-line loading conditions, like the robustness assessment done in [23]. This was done by adjusting the load on Bus 9 and establishing a generating limit for the generators involved in Area 2 to the values given in Table. VIII, thereby adjusting the tie-line power transfer away from its initial value of 400 MW. Figure. 24 displays the results shown in Table. XXV. This test was not feasible for the higher end of tie-line loading on the initial test system for the controls not including an SVC due to the appearance of zero-eigenvalues, meaning the Jacobian matrix has become singular, indicating that the system is on the edge of voltage collapse [22]. A solution for this problem is to reduce the line impedance of the tie-lines, however, this will increase the damping power and hence the damping ratio as discussed in Section. 2.3.5, making the assessment less precise. The maximum tie-line power flow was 815 MW before an unstable mode occurred, however, this was not the mode of interest.

Table XXV
Damping ratio of different control strategies for the inter-area mode with varying tie-line power transfer

	Damping ratio				
Tie line power [pu]	AVR	AVR+PSS	AVR+PSS+SVC	AVR+PSS+SVC +Local input POD	AVR+PSS+SVC +Global input POD
-1	0.05420	0.18230	0.18437	0.17398	0.28137
0	0.04566	0.18466	0.18543	0.17632	0.28275
1	0.03322	0.18045	0.18129	0.17403	0.28534
2	0.02030	0.17265	0.17437	0.17344	0.28643
3	0.008760	0.16331	0.16638	0.17152	0.28311
4	Unstable	0.15481	0.15840	0.16941	0.28041
5	Unstable	0.14261	0.14647	0.15037	0.25832
6	Unstable	0.13447	0.13687	0.13720	0.24358
7	Voltage collapse	Voltage collapse	0.13152	0.12587	0.22519
8	Voltage collapse	Voltage collapse	0.12229	0.11877	0.21068
8.14	Voltage collapse	Voltage collapse	Unstable	Unstable	0.20900

The proposed controller exhibit robustness over a varying range of loading conditions with obvious improvements in response. The weakness for both damping controllers including PODs comes apparent when the tie-line power is adjusted from its initial value. When the tie-line power is reduced, the same proportional increase in damping ratio seen for the control strategies excluding PODs, is not seen for the controllers including PODs. When the tie-line power flow is increased, a slightly higher proportional decrease of damping ratio is observed in the cases including PODs, opposed to those excluding PODs. Retuning the POD for the varying loading conditions may offset the disproportional change in damping ratio. Regardless, the controller including remote signals for the POD showed greater damping ratio for all loading conditions compared to the other control strategies.

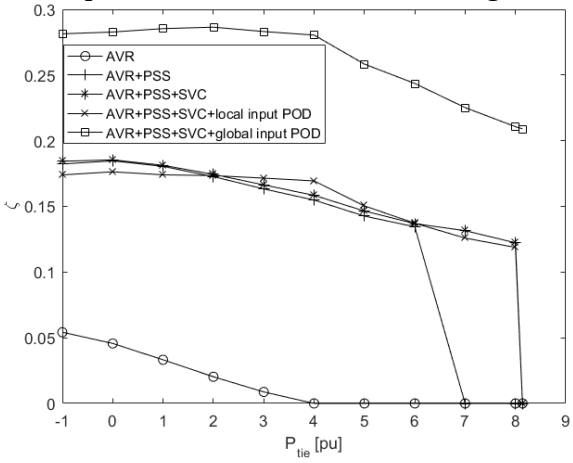

Figure. 24. Damping ratio of different control strategies for the inter-area mode with varying tie-line power transfer

6.6 Robustness assessment 2: transient stability

To further assess the response of the purposed control strategy under severe operating point changes, like sudden load changes or short-circuits, time-domain simulations were performed for the purposed control strategy, as well as the cases in Section. 6.2, 6.3, for reference. The time-domain simulations include a three-phase short circuit on Bus 8 of the test system topology from Figure. 26. The short-circuit have a reactance of $1e^{-5}$ pu and a resistance of 0 pu. The fault take place at t=1.000 s and is cleared at 1.100 s, meaning a duration of 100 ms. The loading conditions are the same as before, i.e., a load of 1767 MW at bus 9, and a tie-line power transfer from area 1 to area 2 of approximately 400 MW. Due to lack of synchronous torque, a simple turbine governor was added to each generator. Their impacts on damping ratio where insignificant, however their presence was crucial for conducting the simulations as oscillatory stable controls lost synchronism following the short circuit. The impact of the turbine governor is best showcased in Figure. 25 a, where the generator clearly is oscillatory unstable and non-oscillatory stable.

Figure. 25 a-e displays the transient damping response of the rotor speed oscillations for generator 1 for the proposed control strategy as well as the test cases, for reference. Each figure title includes the alphabetical identification and what control strategy it represents. The unstable mode of Figure. 25 a is clearly visible. Comparing the local input POD in Figure. 25 d with the controls of Figure. 25 b and c, a slightly better damping is apparent, however, the generator does not reach its initial operating point until the time of 19 s, as the amplitude of delivered synchronous torque of the turbine governor is less, judging by plotting the response of the respective turbine governor. Studying the participation factors, the POD does not significantly participate in the most associated mode of the turbine governor of generator 1 ($\dot{v}_1$=$\dot{v}_2$=0.00004, and $\dot{v}_{\mathrm{POD}}$=0.00014), or the other turbine governors moreover. Its parameters are identical to the other cases and therefore, no explanation can be given for this occurrence. The improved response regarding minimum rotor speed swings is quite apparent for the remote feedback POD in Figure. 25 e. The same problem regarding the slow acting turbine governor is not apparent for this case.

Figure. 26 a-e shows the coherent damping response of the rotor angle oscillations between generator 1 and 3 for each of the simulating cases. The initial rotor angle for the cases including SVC is 0.40631, contradictory to the test cases excluding SVC which is 0.44858 due to different reactive power demands. Reduced amplitude of swings is apparent for the proposed control strategy, with lesser deviation from initial rotor angle. For the proposed control strategy, the greatest amplitude of swings is well below 0.5 referred to the y-axis where the other control strategies go beyond 0.5. Slight improvements in damping are observed for the local input POD in Figure. 26 d compared to the SVC without supplementary control in Figure. 26 c and the PSS case in Figure. 26 b. Oscillatory instability comes quite apparent for the case only including AVR in Figure. 26 a.

Figure. 27 a-e shows the terminal voltage response of generator 1 for each control strategy. Apart from the unstable mode, comparative difference of voltage angle oscillations is slightly apparent only if the plot is comprehensively studied. Therefore, as expected, the proposed control strategy does not have a noteworthy impact on terminal voltage, versus the reference control strategies. PSS design including global signals were shown to improve terminal voltage response following a disturbance on the same test system in [24]. As the PSS has much greater participation on the AVR, it is evident that a PSS designed for damping inter-area oscillations would improve terminal voltage response greater than that of the proposed control strategy. The plot of the AVR-only case in Figure. 27 a illustrates that the AVR is not

able to keep constant terminal voltage following oscillatory instability. Discussed in Section. 2.3.3.2, an increase in rotor speed will cause an approximately decrease in terminal voltage. This is seen comparing Figure. 26.a with 27.a, as the voltage oscillations gradually grows proportional with the growth of rotor speed oscillations. The amplitude of oscillations would be much greater for an equally unstable system with the absence of the AVR.

Figure. 28 a-e shows the active power swing of generator 1 for each control strategy. Figure. 28 a, again shows the lack of damping torque of the AVR-only case. As there was only a slight difference of damping ratio for the cases shown in Figure. 2 b-d, there is only a slight difference of damping response, with the local input POD having slightly improved response when the plot is comprehensively studied. The lesser amplitude of power swings is clear for the proposed control strategy, compared to the reference control strategies.

Lastly, Figure. 29 a-e shows the voltage angle difference between bus 7 and 9. Recalling the system topology from Figure. 22, that is the buses at each end of the tie-lines. The AVR-only case as expected, showed oscillatory instability. Both cases including PODs saw a slight increase in the amplitude of the first swing, however, with faster decaying oscillations. The advantage of the global input POD is quite clear, with fastest decaying oscillations, with respect to the referenced control strategies.

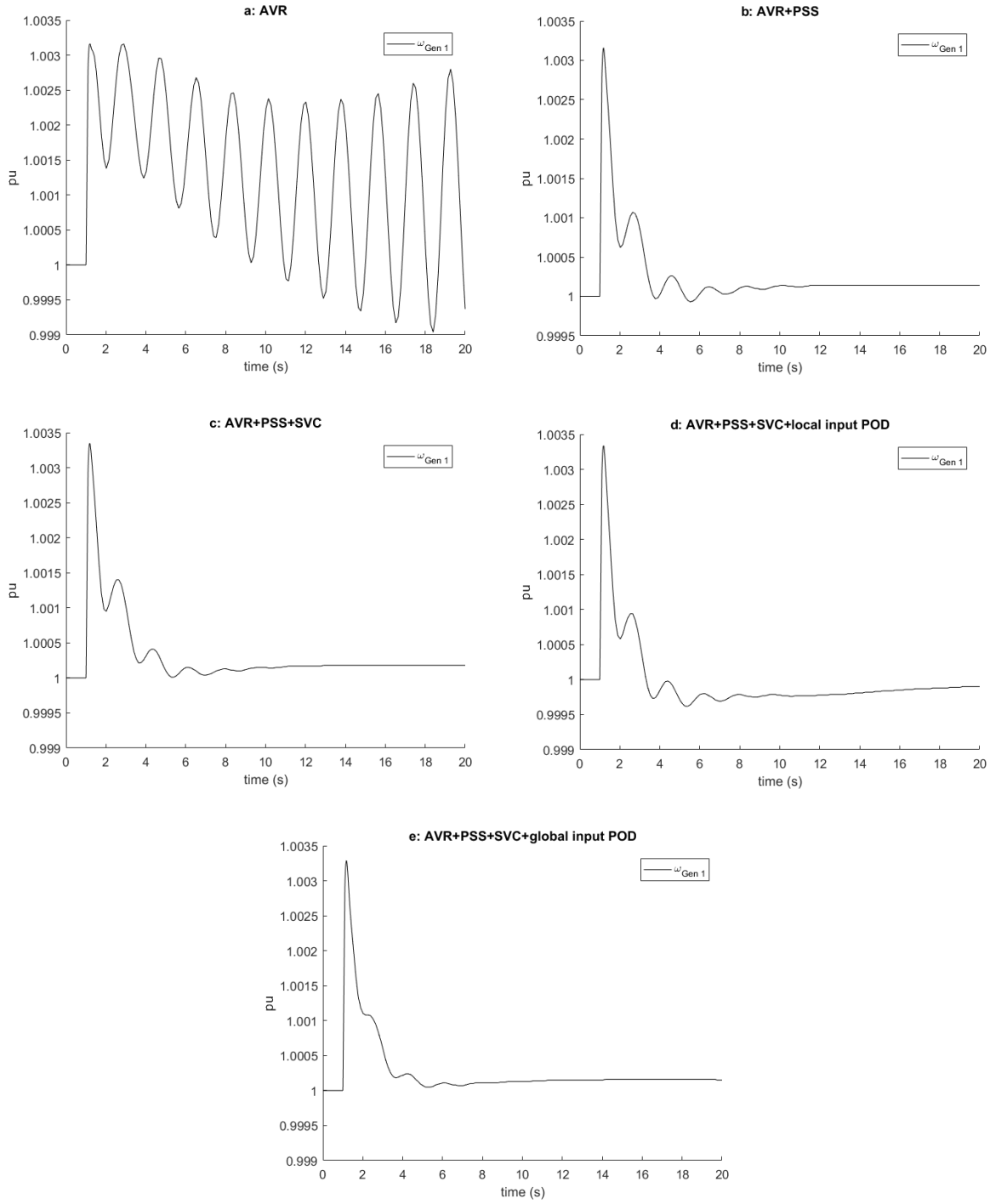

Figure. 25. Transient damping response of the rotor speed oscillations for generator 1

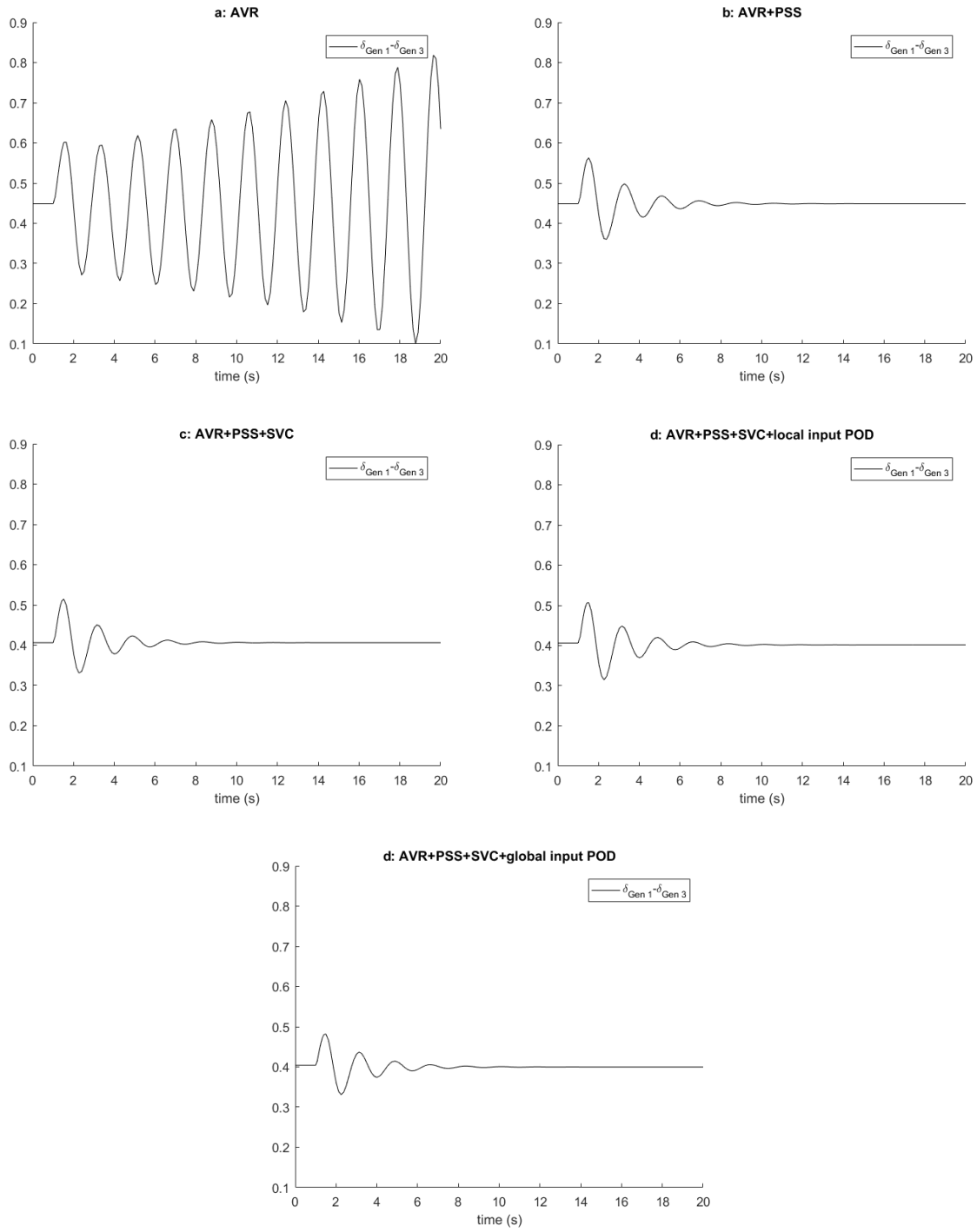

Figure. 26. Coherent damping response of the rotor angle oscillations between generator 1 and 3

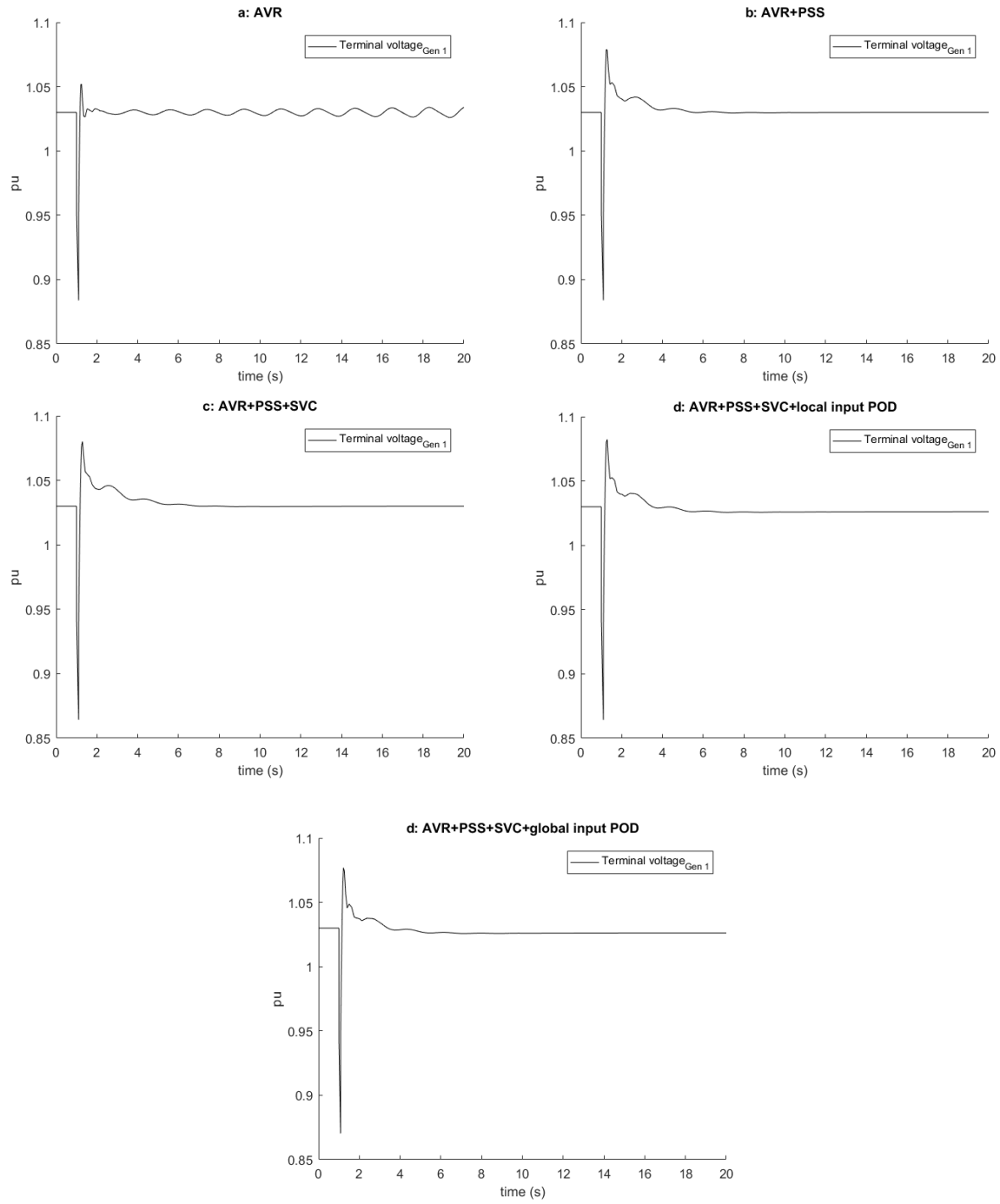

Figure. 27. Terminal voltage response of generator 1

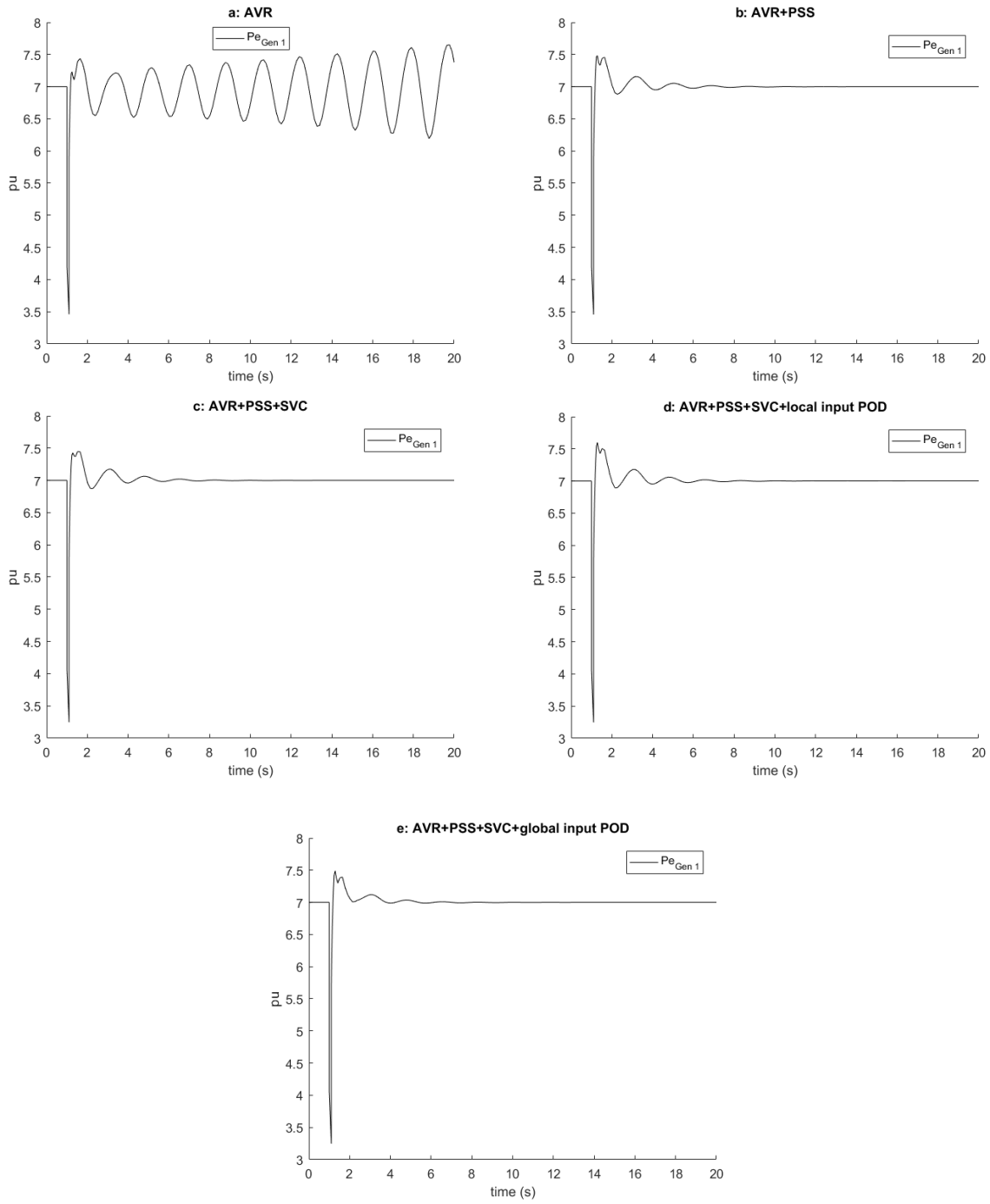

Figure. 28. Active power swing of generator 1

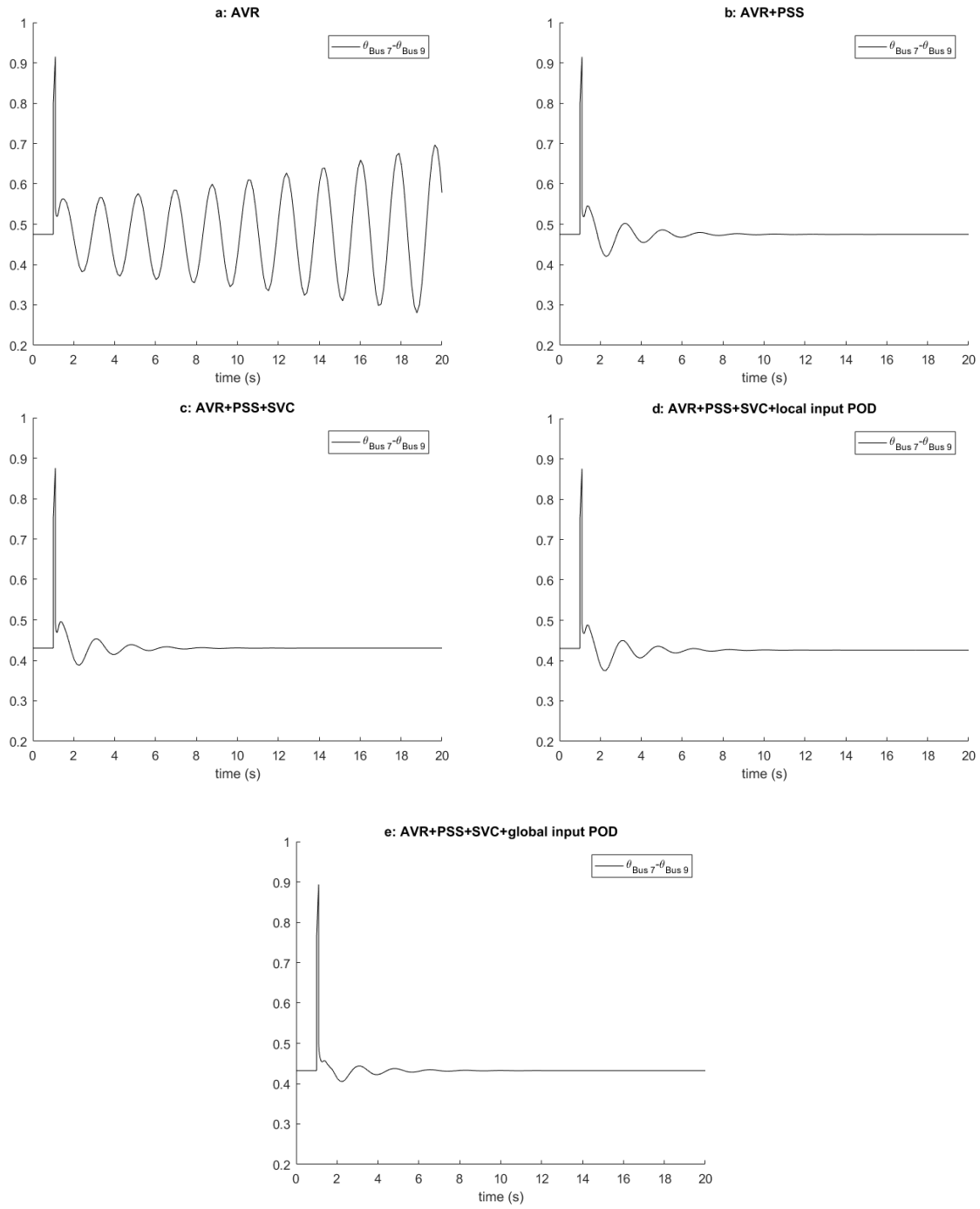

Figure. 29. Voltage angle difference between bus 7 and 9.

7 Conclusion

7.1 Future work

The potential for further research of this specific topic is broad. Future work may include a comparison of different power oscillation damper designs as discussed in Section. 4.2, review of different input signals like those of a power system stabilizer mentioned in Section. 4.3, including a varying time-delay for phasor measurement units discussed in Section. 4.5, application of different FACTS devices and applying the proposed controller and methodology on different test systems suitable for studying inter-area oscillations like the New England IEEE 39-bus system used in [2], or the IEEE 16-machine 5-area system used in [3].

7.2 Summary of results

The aim of this thesis was to implement remote signals from phasor measurement units in a damping controller for inter-area oscillations without decoupling other oscillatory modes of the system. For this reason, the input signals for a power oscillation damper were modified to control a flexible alternating current transmission system device installed on the tie-line, as opposed to employing remote signals on the generators power system stabilizer which has been shown to decrease the damping of local oscillatory modes, as discussed in the Introduction. The goal was to demonstrate that the addition of remote signals can create better damping of inter-area modes than that of a properly tuned local input power oscillation damper, and not worsen the damping of local modes. A methodology based on eigenanalysis was used to site the optimal placement of phasor measurement units, as well as finding the output signal which gives most information about the system which in turn will be the input signal for the power oscillation damper. The siting configuration of the phasor measurement unit, static VAR compensator and power oscillation damper were shown accomplish the goals of improving inter-area damping and stability, without decoupling other modes of oscillations. Lastly, the controller's robustness was put to test proving increased tie-line power transfer capabilities, as well as improving the systems transient stability properties in case of a severe fault.

References

[1] Prabha Kundur, "Power System Stability and Control", published 1994.
[2] F. Liu, R. Yokoyama, Y. C. Zhou, and M. Wu, "TCSC Wide-Area Damping Controller to Enhance the Damping of Inter-area Oscillation for Power Systems with Considering the Time Delay of Wide-Area Signals," in Proc. IEEE Conf. on Power Syst. Techn., 2005, pp. 1-6, 24-28 October.
[3] N. Ray Chaudhuri, S. Ray, R. Majumder, B. Chaudhuri, "A New Approach to Continuous Latency Compensation with Adaptive Phasor Power Oscillation Damping Controller (POD)," IEEE Trans. Power Syst., vol. 25, no. 2, pp. 939–946, May 2010.
[4] N.R. Chaudhuri, A. Domahidi, R. Majumder, B. Chaudhuri, P. Korba, S.Ray, and K. Uhlen, "Wide-area power oscillation damping control in Nordic equivalent system," in IET Gen. Trans. & Dist., vol. 4, no. 10, pp. 1139-1150, 2010.
[5] Y. Zhang, and A. Bose, "Design of Wide-Area Damping Controllers for Interarea Oscillations," IEEE Trans. Power Syst., vol. 23, no. 3, pp. 1136–1143, August 2008.
[6] K. Uhlen, L. Vanfretti, M. M. de Oliveira, B. Leirbukt Member, V. H. Aarstrand, and J. O. Gjerde, "Wide-Area Power Oscillation Damper Implementation and Testing in the Norwegian Transmission Network,"
[7] D.R. Ostojic. "Identification of Optimum Site for Power System Stabiliser Applications," IEEE Proceedings, vol. 135, pt. C, no. 5, September 1988, pp. 416-419.
[8] R. Sadikovi C, "Use Of Facts Devices for Power Flow Control and Damping of Oscillations in Power Systems." PhD Zurich: Swiss Federal Institute of Technology 2006, p. 139
[9] N. Magaji M. W. Mustafa and Z. Bint Muda, "Signals Selection of TCSC Device for Damping Oscillation "
[10] Sudhansu Kumar Samal, Prof. P.C.Panda, "Damping of Power System Oscillations by Using Unified Power Flow Controller with POD and PID controllers", IEEE
[11] Ahad Kazemi Mahmoud, Vakili Sohrforouzani "Power system damping using fuzzy controlled facts devices"
[12] Akhila Sri Tharani, T.R. Jyothsna, "Design of PSS for Small Signal Stability improvement"
[13] Bogdan Marinescu, "Residue phase optimization for power oscillations damping control revisited"
[14] M.A.Furinia, A.L.S.Pereirab, P.B.Araujo, "Pole placement by coordinated tuning of Power System Stabilizers and FACTS-POD stabilizers"
[15] Julio C. R. Ferraz, Member, IEEE, Nelson Martins, Fellow, IEEE and Glauco N. Taranto, Member, IEEE, "Coordinated Stabilizer Tuning in Large Power Systems Considering Multiple Operating Conditions"
[16] Y.F. Lin, Z. Xu, Member, IEEE Y. Huang, "Power oscillation damping controller design for TCSC based on the test signal method"
[17] A. Simdes Casta, F. D. Preitas, and A. S. Silva, "Design of decentralized controllers far large power systems considering sparsity,"
[18] Antonio L. B. do Bomfim, Glauco N. Taranto, Member, IEEE, and Djalma M. FalcBo, Senior Member, IEEE, "Simultaneous tuning of power system damping controllers using genetic algorithms"
[19] Narayan Nahaka Ranjan, Kumar Mallick, "Damping of power system oscillations by a novel DE-GWO optimized dual UPFC controller"
[20] J. W. Stahlhut, T. J. Browne, G. T. Heydt, and V. Vittal, "Latency viewed as a stochastic process and its impact on wide area power system control signals,"

[21] G.C. Verghese, I.J. Perez-Arriaga, and F.C. Schweppe, “selective modal analysis with application to electric power systems” IEEE Trans., Vol., PAS-101, No. 9, pp. 3117-3134, September 1982.
[22] Ian Dobson, Liming Lu, "Voltage Collapse Precipitated by the Immediate Change in Stability When Generator Reactive Power Limits are Encountered", IEEE Transactions on Circuits and Systems I Fundamental Theory and Applications 39(9):762 – 766
[23] Abdlmnam Abdlrahem1, Parimal Saraf, Karthikeyan Balasubramaniam, Ramtain Hadidi, Alireza Karimi, Elham Makram, "Design of a Fixed‐Order Robust Controller to Damp Inter‐Area Oscillations in Power Systems"
[24] Aaron Francis Snyder, "Inter-Area Oscillation Damping with Power System Stabilizers and Synchronized Phasor Measurements".
[25] M.E. About-Ela, A.A. Sallam, J.D. McCalley and A.A. Fouad. “Damping Controller Design for Power System Oscillations Using Global Signals,”
[26] Jan Machowski, Janusz W. Bialek, James R. Bumby, "POWER SYSTEM DYNAMICS Stability and Control, Second Edition".
[27] Debasish Mondal, Abhijit Chakrabarti and Aparajita Sengupta, "Power System Small Signal Stability Analysis and Control".
[28] O.G.C. Dahl, "ELECTRIC POWER CIRCUITS Theory and Applications, Volume II, Power System Stability".
[29] Phadke, A.G., Thorp, J.S., "Synchronized Phasor Measurements and Their Applications".
[30] M. Klein, G.J. Rogers Senior member IEEE, P. Kundur fellow IEEE, "A FUNDAMENTAL STUDY OF INTER-AREA OSCILLATIONS IN POWER SYSTEMS", Transactions on Power Systems, Vol. 6, No. 3, August 1991
[31] Samima Akter, Anulekha Saha, Prof. Priyanath Das, "Modelling, Simulation and Comparison of Various FACTS Devices in Power System"
[32] Reena Singh, Pallavi Bondriya, Mitali Kushwaha, "ANALYSIS AND COMPARISON OF VARIOUS FACTS DEVICES"
[33] Prof. Mohamed EL-Shimy, answer #2
https://www.researchgate.net/post/how_to_use_function_fm_abcd_in_PSAT_toolbox
[34] IEEE Power Engineering Society System Oscillations working group, “Inter-area Oscillations in Power Systems”
[35] https://www.electrical4u.com/lenz-law-of-electromagnetic-induction/
[36] https://www.electrical4u.com/faraday-law-of-electromagnetic-induction/
[37] Federico Milano, "Power System Analysis Toolbox: Documentation for PSAT version 2.0.0”, February 14, 2008

Appendix A: Description of matrix structure in PSAT

The command "fm_abcd" computes the whole state space model for the multiple input multiple output (MIMO) system and stores them in a structure called "LA".

The **A**-matrix is stored in "LA.a" and contains the full state matrix of the system

The input matrix **B** is constructed by the various control devices. The SVC- and AVR-devices create a nx1 contribution to the **B**-matrix as they are inputs. For example, the **B**-matrix for the AVR-unstable system in Section. 6.2 is of the dimension 36x4, since the system contains 4 AVRs and its state matrix is of the dimension 36x36. The **B**-matrix of the system containing AVR+PSS+SVC similarly in section. 6.2 is of the dimension 49x5, since the SVC also contributes to the **B**-matrix.

The **C**-matrix stored as LA.c_y is the output matrix for the entire MIMO system, while only a specific part of this matrix is required based on the selected inputs to the controller. For finding the corresponding **C**-matrix, LA.c_y must be combined with the transfer matrices. The transfer matrices can be expressed in sending- and receiving-end current, real power, and reactive power. The combined **C**-matrix is of the dimension (number of lines)xn. For example, if the sending end real power is the exciting input quantity, then the corresponding **C**-matrix can be obtained using C=LA.h_ps*LA.c_y, where LA.h_ps means sending end power in the output vector. Recieving end power would be LA.h_pr. PSAT cannot directly provide the transfer matrices for sending- and recieving-end voltage, however, these matrices can easily be calculated from the transfer matrices provided. In Section. 6.2, 6.3 and 6.4, the bus voltage transfer matrix was needed for obtaining the **C**-matrix. This was calculated using the recieving end current, real power and reactive power matrices. For example, the row corresponding to the receiving end voltage for line 6-7 represent the bus voltage for Bus 7.

The **D**-matrix was 0 for all cases tested, likely due to the use of open loop transfer functions [33].

Appendix B: Description of generator modelling

Since the synchronous generator is victim of oscillations, a brief explanation will be provided of the sixth order synchronous generator, and dq-transformation with notations from [1].

For balanced operation, the armature mmf wave appears stationary with respect to the rotor and has approximately sinusoidal distribution. A sine function can be expressed as a sum of two sine functions. Therefore, the mmf from the stator windings can be resolved into two sinusoidally distributed mmf waves stationary with respect to the rotor, so that one has its peak over the d-axis and one over the q-axis [26]. A visual presentation of this is shown in Figure. B1. All generator windings are magnetically coupled so that the flux in each winding depends on the current in all the other windings. Also, the mutual inductances are subject to periodic changes due to rotation of the rotor and saliency. By establishing three sets of fictitious perpendicular windings representing the armature of the synchronous generator from the dq0-frame, all elements of inductance become constant and independent of time as the dq0-frame is constantly rotating with the magnetic rotor axis [26]. This transformation makes state-space representation possible and will therefore be explained. The machine has one d-axis field winding, one d-axis damper winding and two q-axis damper windings. For system analysis a limited number of circuits is sufficient, but for machine design analysis, more circuits may be used for increased accuracy [1]. The 0-axis will be omitted as no current is induced here during steady-state operation.

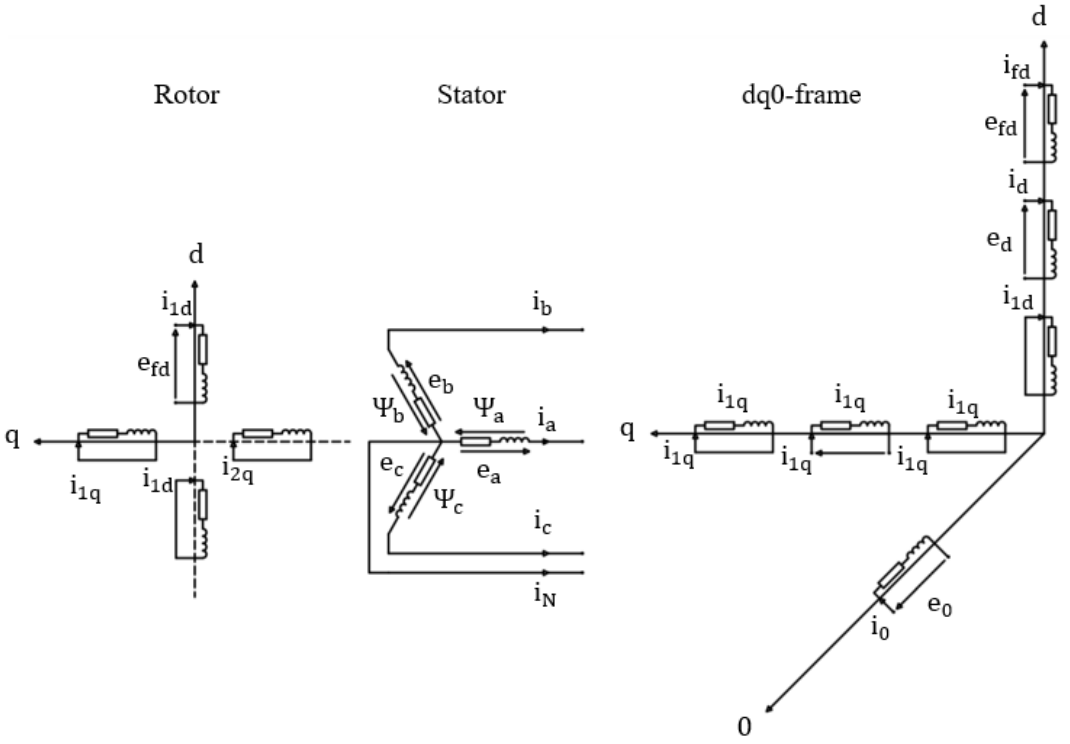

Figure B1. Rotor and stator circuits of a synchronous generator in standard- and rotor reference frame

The transformation mapping the synchronous generator to the rotating reference frame is called Park's transformation, and is given by the rotating matrix

$$P_s = \frac{2}{3}\begin{bmatrix} \cos\theta & \cos\left(\theta - \frac{2\pi}{3}\right) & \cos\left(\theta + \frac{2\pi}{3}\right) \\ \sin\theta & \sin\left(\theta - \frac{2\pi}{3}\right) & \sin\left(\theta + \frac{2\pi}{3}\right) \\ \frac{1}{2} & \frac{1}{2} & \frac{1}{2} \end{bmatrix} \tag{5.1}$$

The dq-equivalent circuit is given in Figure. B2.

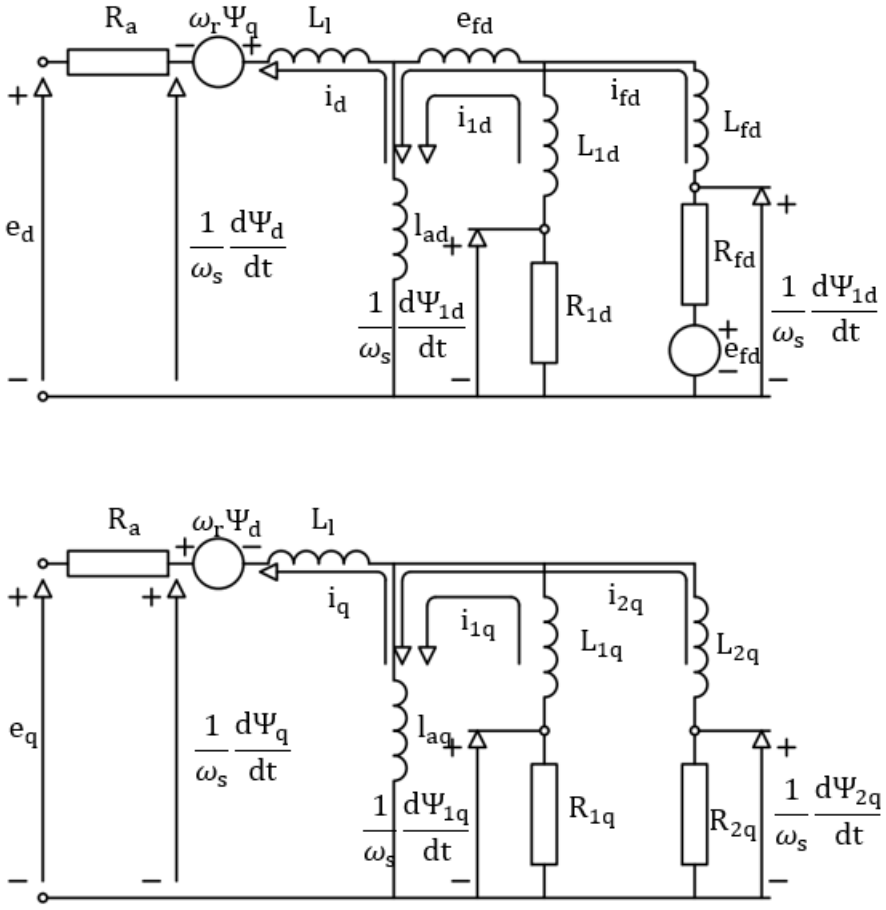

Figure. B2. Dq-equivalent circuits for the synchronous machine.

The stator voltage equations are given by

$$e_d = \frac{1}{\omega_s}\frac{d\Psi_d}{dt} - \Psi_q\omega_r - R_a i_d \tag{5.2}$$

$$e_q = \frac{1}{\omega_s}\frac{d\Psi_q}{dt} + \Psi_d\omega_r - R_a i_q \tag{5.3}$$

$$e_0 = \frac{1}{\omega_s}\frac{d\Psi_0}{dt} - R_a i_0 \tag{5.4}$$

Note the signs associated with the speed voltage terms. Since it is assumed the q-axis lead the d-axis by $\pi/2$, the voltage e_q is induced by the flux in the d-axis. Likewise, the voltage e_d is induced by a flux in an axis lagging the d-axis by $\pi/2$, i.e., the negative q-axis. Consequently, the voltage induced in the q-axis due to rotation is $+\Psi_d\omega_r$ and that in the d-axis is $-\Psi_q\omega_r$. Since the 0-axis is perpendicular to the d- and q-axis, no voltage is induced due to rotation of these axes.

The rotor voltage equations are given by

$$e_{fd} = \frac{1}{\omega_s}\frac{d\Psi_{fd}}{dt} + R_{fd}i_{fd} \tag{5.5}$$

$$0 = \frac{1}{\omega_s}\frac{d\Psi_{1d}}{dt} + R_{1d}i_{1d} \tag{5.6}$$

$$0 = \frac{1}{\omega_s}\frac{d\Psi_{1q}}{dt} + R_{1q}i_{1q} \tag{5.7}$$

$$0 = \frac{1}{\omega_s}\frac{d\Psi_{2q}}{dt} + R_{2q}i_{2q} \tag{5.8}$$

Figure. B3 show an equivalent circuit representing the d- and q-axis stator and rotor flux linkages, with the currents appearing as loop currents. This figure represents the flux linkage equations (5.9), (5.10), (5.12), (5.13), (5.14), and (5.15). The stator flux linkage equations are given by

$$\Psi_d = -(L_{ad} + L_l)i_d + L_{ad}i_{fd} + L_{ad}i_{1d} \tag{5.9}$$

$$\Psi_q = -\left(L_{aq} + L_l\right)i_q + L_{aq}i_{1q} + L_{aq}i_{2q} \tag{5.10}$$

$$\Psi_0 = -L_0 i_0 \tag{5.11}$$

The rotor flux linkage equations are given by

$$\Psi_{fd} = L_{fdfd}i_{fd} + L_{fd1d}i_{1d} - L_{ad}i_d \tag{5.12}$$

$$\Psi_{1d} = L_{fd1d}i_{fd} + L_{1d1d}i_{1d} - L_{ad}i_d \tag{5.13}$$

$$\Psi_{1q} = L_{1q1q}i_{1q} + L_{aq2q}i_{1d} - L_{aq}i_q \tag{5.14}$$

$$\Psi_{2q} = L_{aq}i_{1q} + L_{2q2q}i_{2q} - L_{aq}i_q \tag{5.15}$$

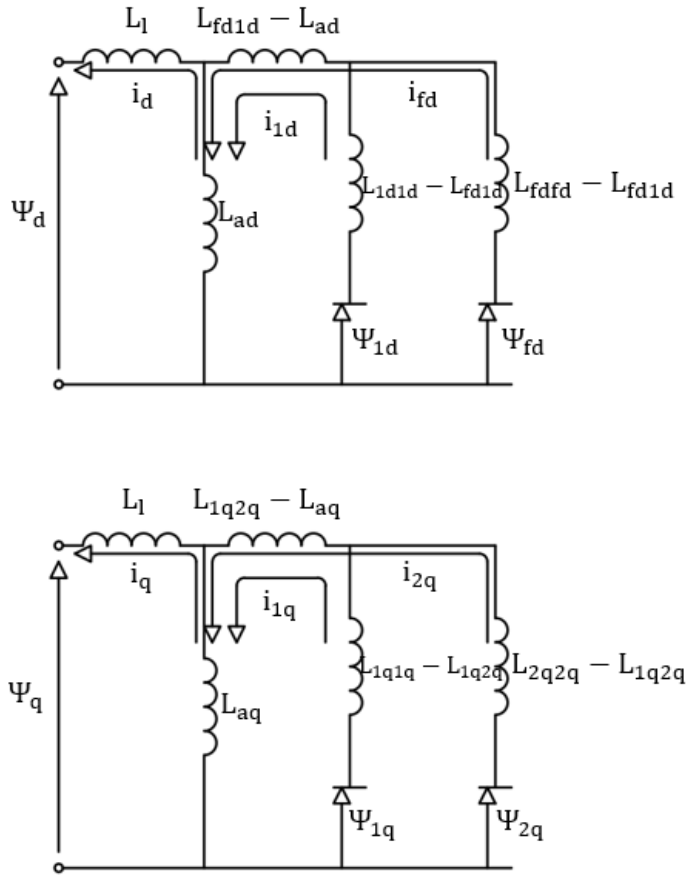

Figure. B3. dq-representation of rotor and stator flux linkages

Self-explanatory, the inductances containing two dissimilar elements in the subscript is the mutual inductance between the before-mentioned windings, e.g., L_{fd1d} is the mutual inductance between the field winding and the d-axis damper winding. Similarly, the inductances containing two similar elements in the subscript is the self-inductance of that winding.

The machine model is developed assuming linear coupled circuits, i.e., linear flux-current relationships. This is so the superposition principle is applicable. Magnetic saturation of the rotor and stator is, however, of great importance. The equivalent circuit identifying nonlinear elements in the d- and q-axis and air gap flux linkages, as well as the representation of saturation characteristics is shown in Figure. B4. The model assumes the leakage inductances are independent of saturation, the leakage fluxes do not contribute to iron saturation, the saturation relationship between the resultant air gap flux and the mmf is independent of load, and that there is no magnetic coupling between the d- and q-axes as a result of nonlinearities introduced by saturation.

The saturation equations are given by

$$\Psi_{ad} = \Psi_d + L_l i_d \tag{5.15}$$

$$\Psi_{aq} = \Psi_q + L_l i_q \tag{5.16}$$

$$\Psi_{at} = \sqrt{\Psi_{ad}^2 + \Psi_{aq}^2} \tag{5.17}$$

$$L_{ad} = f(\Psi_{at})L_{adu} \tag{5.18}$$

$$L_{aq} = f(\Psi_{at})L_{aqu} \tag{5.19}$$

where Ψ_{ad} and Ψ_{aq} is the d- and q-axis air-gap flux linkage, and Ψ_{at} is the air gap flux linkage. L_{adu} and $L_{aqu}$is the d- and q-axis unsaturated mutual stator inductance.

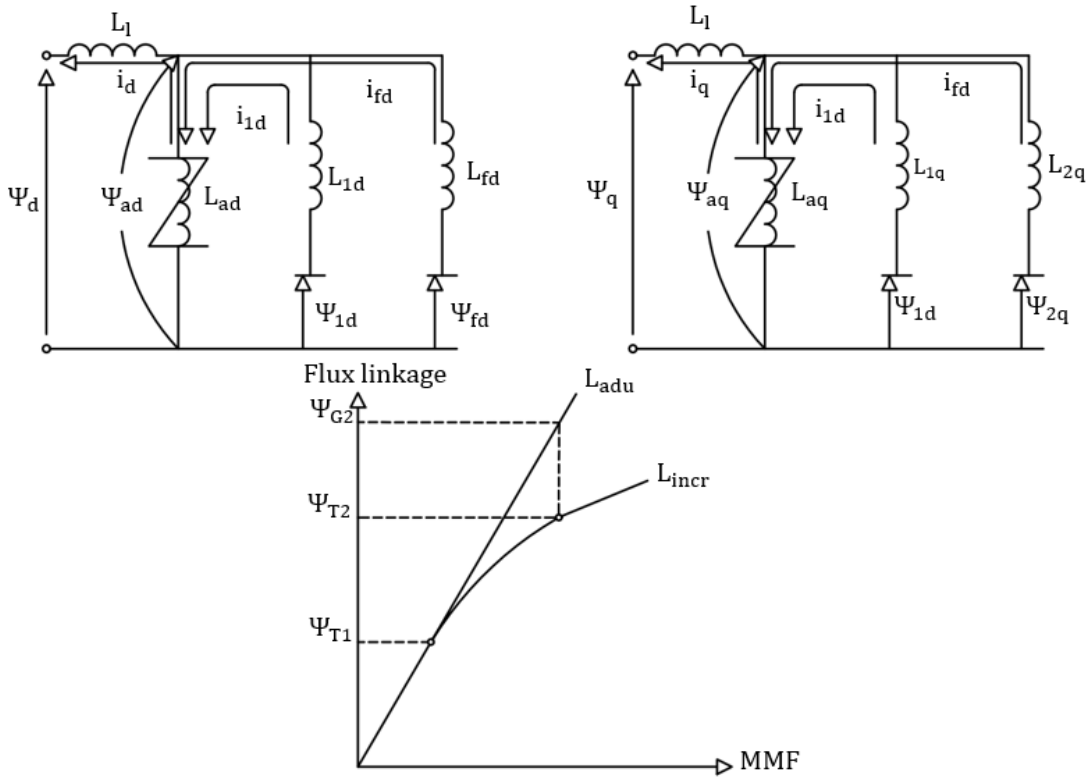

Figure. B4. dq-equivalent circuits representing non-linearities and air-gap flux linkages. The graph represents open-circuit characteristics showing effects of saturation.